

**WIND, THERMAL, AND EARTHQUAKE MONITORING  
OF THE WATTS TOWERS:  
PRELIMINARY RESULTS-DRAFT 1**

Jackson English  
Ertugrul Taciroglu  
Robert Nigbor

University of California, Los Angeles  
Department of Civil & Environmental Engineering

UCLA - SGEL  
Report 2013/01



## FUNDING AGENCY ACKNOWLEDGMENT AND DISCLAIMER



Funding for this work was provided by the National Science Foundation through Award CMMI-1331299 with collaboration by the George E. Brown Network for Earthquake Engineering Simulation under Award CMMI-0927178. Any opinions, findings, and conclusions or recommendations expressed in this material are those of the author(s) and do not necessarily reflect the views of the National Science Foundation.

Executive Summary .....	v
1 Introduction .....	6
2 Instrumentation .....	7
3 Preliminary Data Collection Results .....	11
3.1 COMPARISON OF LACMA AND UCLA WEATHER DATA .....	11
3.2 EFFECTS OF TEMPERATURE ON FUNDAMENTAL FREQUENCY .....	12
3.3 DAILY TILT CYCLES .....	15
3.4 EARTHQUAKE AND WIND RESPONSE.....	20
3.5 CRACK DISPLACEMENT .....	25
3.6 EAST TO CENTER TOWER COUPLED MOTION.....	31
4 Computer Modeling .....	36
4.1 LIDAR SCAN.....	36
4.2 DEFINING MODEL GEOMETRY .....	37
4.3 ESTIMATION OF STRUCTURAL PROPERTIES.....	41
4.4 INITIAL MODEL RESULTS .....	44
4.5 THERMAL SIMULATIONS.....	45
5 Summary .....	47
References.....	50

Figure 2.1: Location of Accelerometer and Tilt Meter .....	8
Figure 2.2: (A) Triaxial Accelerometer and (B) Biaxial Inclinometer .....	8
Figure 2.3: (A) North and (B) South Side Crack Displacement Sensors .....	9
Figure 2.4: Wind Sensor .....	9
Figure 3.1: LACMA vs UCLA Temperature Comparison .....	11
Figure 3.2: LACMA vs UCLA Wind Speed Comparison .....	12
Figure 3.3: Acceleration Power Spectral Density .....	13
Figure 3.4: Frequency Variation with Temperature over Time .....	13
Figure 3.5: January - May Frequency vs Temperature .....	14
Figure 3.6: Frequency Histogram.....	14
Figure 3.7: February Tilt.....	15
Figure 3.8: Average Daily Temperature versus Peak Daily Tilt .....	17
Figure 3.9: Band-pass Filtered February Tilt.....	17
Figure 3.10: Week of 2/01/13 Tilt vs Azimuth Angle .....	18
Figure 3.11: Daily Tilt Cycles (A) Month of February (B) Sunrise (C) Noon (D) Sunset .....	19
Figure 3.12: Earthquake Acceleration Response .....	21
Figure 3.13: Earthquake Tilt Response .....	21
Figure 3.14: Earthquake Crack Response .....	22
Figure 3.15: Wind Speed and Direction .....	23
Figure 3.16: Wind Storm Acceleration Response .....	23
Figure 3.17: Wind Storm Tilt Response .....	24
Figure 3.18: Wind Storm Crack Response .....	24
Figure 3.19: Crack Displacement Sensor Locations .....	25
Figure 3.20: LACMA vs UCLA North Crack Displacement.....	26
Figure 3.21: LACMA vs UCLA South Crack Displacement.....	26
Figure 3.22: North and South Crack Displacement for 4/12 and 4/17 .....	27
Figure 3.23: Peak Daily Solar Radiation .....	28
Figure 3.24: Selected Daily Crack Displacement for High and Low Solar Radiation Days.....	29
Figure 3.25: Shade Experiment Setup .....	30
Figure 3.26: Shade Experiment Crack Displacement .....	30
Figure 3.27: Coupled Motion Sensor Arrangement .....	31
Figure 3.28: East-West Acceleration Transfer Between Towers .....	32
Figure 3.29: North-South Acceleration Transfer Between Towers.....	32
Figure 3.30: East Tower Power Spectral Density .....	33
Figure 3.31: West Tower Power Spectral Density .....	34
Figure 3.32: Log Decrement Damping Approximation.....	35
Figure 4.1: LIDAR Scan of the Watts Towers Site .....	36
Figure 4.2: Tower Member Labels .....	37
Figure 4.3: Laser Scan Horizontal Section Cut Showing Column Locations .....	38
Figure 4.4: Sample Column Location Spreadsheet .....	39
Figure 4.5: Vertical Section Cut Showing Band Cross-Sections .....	40
Figure 4.6: ASCE 41-06 Table 6.3. Default Lower-Bound Compressive Strength of Concrete (psi) .....	41
Figure 4.7: A) Finished Model B) N-S First Mode Shape C) E-W First Mode Shape.....	44

# Executive Summary

# 1 Introduction

The Watts Towers site consists of 17 interconnected structures that were constructed over a 34-year period between 1921 and 1955 by a single artist, Simon Rodia. The most distinct features of the site are the three towers, two of which are almost 100 feet in height.

Preservation efforts on the Watts Towers date back to 1959. When the City of Los Angeles ordered the compound to be demolished at the time, two individuals purchased the property, and the Committee for Simon Rodia's Towers in Watts (CSRTW) was formed, which included a curator of the Los Angeles County Museum of Art (LACMA). This committee reached an agreement with the City of Los Angeles to carry out loading tests to assess the safety of the structures.

Even during construction of the Towers, there were indications of decay, and reportedly, Rodia constructed new elements while repairing the existing structures (Goldstone, 1997, p. 53). While the structural frame is generally deemed stable and sound, there are numerous locations where the cement cover has cracked. Decorative ornaments likewise have formed cracks and become detached. Several major restoration attempts have been made to date, often in response to disasters such as the Northridge earthquake in 1994 and a major rainstorm in 2008.

The condition of the Watts Towers was previously reviewed by an engineering firm (Ehrenkrantz) in 1983; and this study resulted in the development of a "Conservation Handbook." This guideline document prescribed a variety of intervention methods, which were aimed at repairing the damage and slowing the deterioration of the structural frame. In 1988 and 1989, ANCO Engineers carried out an environmental study aimed at addressing the causes for the extensive cracking. In 2004-2005, the Architectural Resources Group (ARG) undertook a study of the cracks and an evaluation of repair methods and materials. More recently, LACMA has partnered with the City of Los Angeles' Department of Cultural Affairs, with the objective of developing a comprehensive long-term preservation plan for the Watts Towers. Since 2011, LACMA's Conservation Center had been working towards the stated goal.

While the aforementioned efforts have yielded a guideline document for the preservation of Watts Towers—*viz.*, the aforementioned Conservation Handbook—, a long-term strategy is still lacking. The most visible manifestations of the deterioration of the towers are cracks in the cement plaster and loss of ornamental decoration. Multiple repair attempts in the past were unsuccessful, and the cracks kept reappearing. Corrosion of the metal armature has always been considered to be the main cause of the deterioration, but mechanical stresses were never fully taken into consideration in prior studies, despite the observation that increased damage was observed after every heavy wind storm. The potential effects of thermal stresses were ignored as well.

LACMA's main task at the present time is to review and to revise the "Conservation Handbook," which guides all physical interventions at the Towers. For the said revision, the LACMA conservators find it necessary to better understand all the factors contributing to the deterioration and to understand the reasons underlying the failure of past interventions. Preliminary studies—carried out and/or commissioned by LACMA—based on limited sensor readings indicated that:

1. Cracks are opening and closing on a daily basis as a result of thermal stresses.
2. Santa Ana winds can create quasi-static and dynamic loadings comparable to a seismic event.
3. Santa Ana winds can lead to irreversible widening of cracks

Santa Ana winds are seasonal, strong (nominally > 40 mph and sometimes reaching above 80 mph), and persistent (northerly at the site) downslope winds that affect Southern California.

Invited by the LACMA conservation team lead by Dr. Frank Preusser, the UCLA team has been studying the global structural behavior of the Watts Towers, including the collection of data on structural responses (accelerations and crack displacements) and environmental loads (temperature, wind speed, wind direction) since January 30, 2013. This report serves as a summary of the work completed thus far, and highlights some of the key preliminary findings. The towers will remain instrumented until December 2013. Once the data collection and analysis is complete, this report will be updated with a set of final conclusions.

## **2 Instrumentation**

In order to analyze the behavior of the Central Tower, several different sensors were used, including accelerometers, inclinometers, displacement sensors, dynamic wind sensors and temperature sensors.

The accelerometers are all EpiSensor ES-T models, designed and produced by Kinemetrics (Kinemetrics). The triaxial EpiSensor force-balance accelerometers combine a wide frequency and acceleration range with a very low noise level. This allows for accurate vibration measurements at amplitudes below  $\mu\text{g}$ 's. One accelerometer was placed on the north side of the Central Tower, approximately 23 feet above the ground. An additional accelerometer was placed on the ground 90 feet to the west of the Center Tower. The accelerometers record ambient, earthquake and wind induced vibrations, and allow for estimation of modal frequencies.

An inclinometer was used to track the motion of the tower. This device is a precision biaxial tiltmeter (model 716-2B) from Applied Geomechanics (Applied Geomechanics), which was attached at the same location as the accelerometer. This model of tiltmeter is accurate down to approximately  $1 \mu\text{rad}$ . The tiltmeter also includes an internal thermometer, which was used for the initial stages as an estimate of the ambient and surface temperatures.



Figure 2.1: Location of the accelerometer and the tilt meter



Figure 2.2: (A) Triaxial accelerometer and (B) biaxial inclinometer

To directly measure the crack movements, two cable-position transducers, Model 150 from Firstmark Controls (Firstmark Controls), were placed over existing cracks. Unlike traditional string potentiometers that are primarily used for static or quasi-static displacement readings, the design of this sensor allows it to capture small amplitude static and dynamic displacements. These sensors are accurate down to a very low level, and are capable of capturing movements on the scale of 1  $\mu$ inch. The crack sensors provide data on how the cracks open and close over the course of the day, whether or not the crack is continuing to open over time, and what effects, if any, earthquakes and wind have on crack movement.



Figure 2.3: (A) North and (B) south side crack displacement sensors

Wind speed, wind direction, and ambient temperature were recorded using an ultrasonic anemometer, Model WindObserver 65 by Gill Instruments (Gill Instruments). The sensor was mounted approximately 10 feet off of the north side of the center tower and 15 feet off the ground. This positioning allows the sensor to get a clean reading, free from most of the turbulent zones created by the towers or the surrounding walls. This sensor can measure dynamic components of wind gusts to about 5 Hz, and so will be a proxy for dynamic wind loads on the central tower.

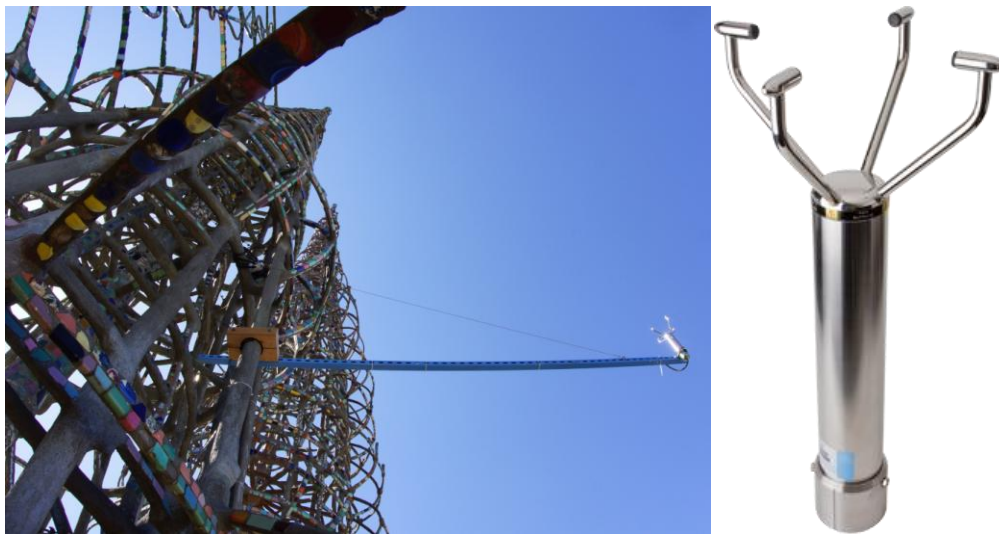


Figure 2.4: Wind sensor

The sensors were all connected to Quantera Q330 data-loggers (Quantera). The Q330 features high-resolution 24-bit A/D conversion and GPS time stamping that is accurate down to a microsecond. Each Q330 has only 6 channels of input, but the GPS time stamping allows for synchronization across multiple digitizers. Data were sampled continuously at 200 Hz and saved to a new output file at the beginning of each hour.

In addition to the sensors mentioned above, LACMA previously installed a weather station on top of the storage trailer that is located at the northwest corner of the site, and crack displacement sensors at three different locations on the Central Tower. The LACMA weather

station features additional useful information, such as humidity and solar radiation, which help to better understand the environmental conditions.

The sensors were deployed in different phases, with new sensors being added as they became available or were deemed necessary. The first phase consisted of only the accelerometer and tiltmeter, and lasted from January 30 to March 11, 2013. Phase two added the two crack displacement sensors and the wind sensor. Although the crack sensors were installed on March 11, they were initially using the Q330 as a power supply, which introduced significant amounts of noise into the data. It wasn't until they were hooked up to a regulated power supply on April 8 that the crack displacement data were considered usable for the small daily movement. The third phase started on May 10 when the tiltmeter was removed and the ground accelerometer was added.

During the week of July 29, additional trials were completed with the help of an articulated boom truck. The truck allowed the placement of sensors at previously unreachable heights. Two different arrangements of sensors were used. The first trial consisted of placing two accelerometers on the Central Tower at heights of 45 and 53 feet, one accelerometer on the East Tower at 33 feet, and one sensor on the West Tower at 34 feet. A second trial was completed with all four of the new accelerometers on the Central Tower at heights of 10.5, 31, 45 and 53 feet.

### 3 Preliminary Data Collection Results

Sampling data at 200Hz is necessary in order to accurately capture short-term dynamic motions of the tower. In order to study the long-term response of the tower to the environment, the tilt, temperature, and crack displacement data were all averaged within each one-hour block. The one-hour averaged data are what will be presented in this chapter unless otherwise noted. The tilt and crack data were further processed, in order to normalize their baseline values to zero.

#### 3.1 Comparison of LACMA and UCLA Weather Data

Since both the LACMA and UCLA weather station data will be used to examine various trends, it is first necessary to see how they compare to each other and verify that the recorded values for temperature and wind speed are reasonably close.

The LACMA station records the weather data at one sample every five minutes. To facilitate a one to one comparison, the UCLA data were resampled at the five-minute rate. The one-hour average temperature values from the tilt meter are included as well.

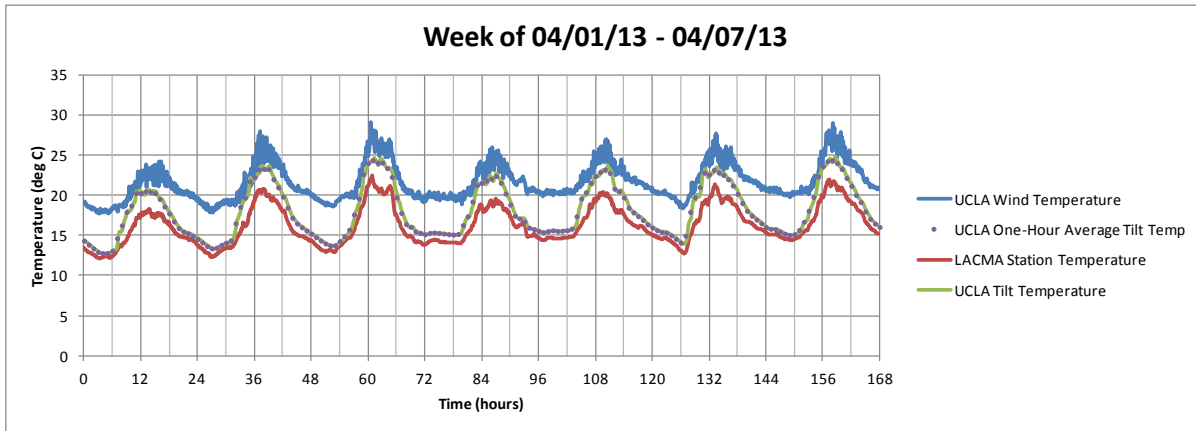


Figure 3.1: LACMA vs UCLA temperature comparison

The highest temperature values come from the wind sensor, followed by the tiltmeter, and with the LACMA station reading the lowest values. On average, the tiltmeter and the wind sensor record 1.7°C and 5.4°C higher temperature values than the LACMA station, respectively. Another thing to note is that the one-hour average temperature values follow the same trend as the 5-minute sampling—accurately capturing the peaks and valleys throughout the day.

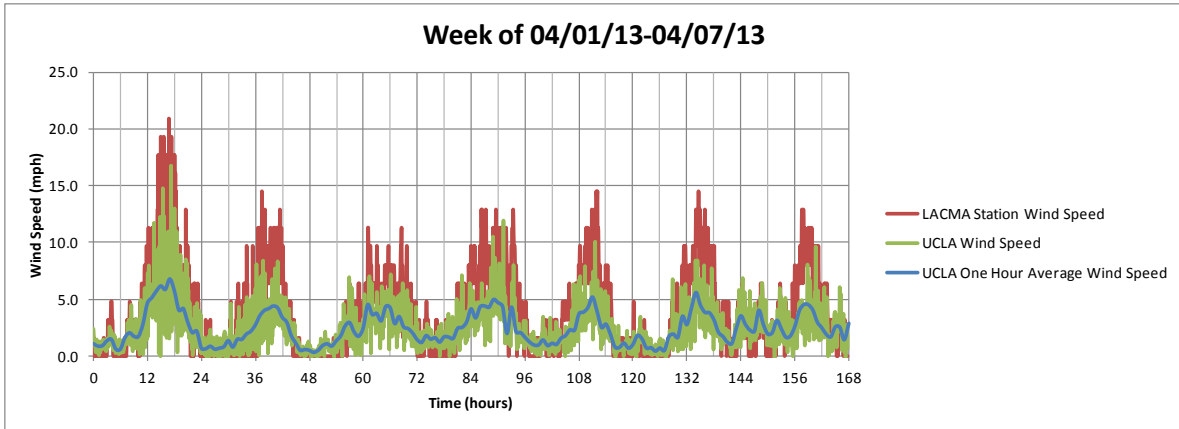


Figure 3.2: LACMA vs UCLA wind speed comparison

Opposite of the temperature data, the LACMA weather station records higher values for wind speed than the sensor attached off of the tower. The wind speed recorded by the UCLA sensor is 1.4 mph less, on average, than the LACMA station. Taking the one-hour average of the wind speed leads to a large decrease in the peak values. Peak wind speed, unlike temperature, is often registered as gusts during relatively short periods of time. The gusts are averaged out when looking at a full hour. Even the five-minute sampling rate leads to an underestimation of peak speeds. At hour 18 (6 pm on 4/01) the five-minute data give a peak value of 15 mph, whereas the actual peak wind gust was around 23 mph. These data nonetheless tell the story of when wind speeds peaked. During periods with strong gusts, the full data set can be analyzed for short-term trends.

A comparison of the LACMA and UCLA crack displacement data will be presented in section 3.5.

### 3.2 Effects of Temperature on Fundamental Frequency

The frequency of a structure is an important response parameter as it provides an estimate of the structure's global stiffness. In structural health-monitoring studies, the frequency is often calculated before and after an event with the anticipation that any damage to a key structural members will cause cracking or the loosening of connections, which will result in a lower stiffness. If the frequency of a structure is significantly lower following an event, then it is likely that there has been some damage. The frequency of a structure is also dependant on various environmental conditions.

The first three frequencies of the Central Tower are easily identifiable by finding the averaged power spectral density of the acceleration signal. The function `pwelch` was used in Matlab, which returns the estimated PSD using Welch's averaged modified periodogram method (MATLAB, 2013). The function defaults to using an average of 8 windows with a 50% overlap. To increase accuracy, the window size was set to 20,000 points, which results in a one-hour file being subdivided into 36 equal windows. The same 50% overlap between windows was used. By plotting the resulting power density versus frequency, it is easy to identify the first three modes, as shown below. A simple method of peak-picking was used here to obtain the dominant natural frequencies (cf. circled locations in the figure).

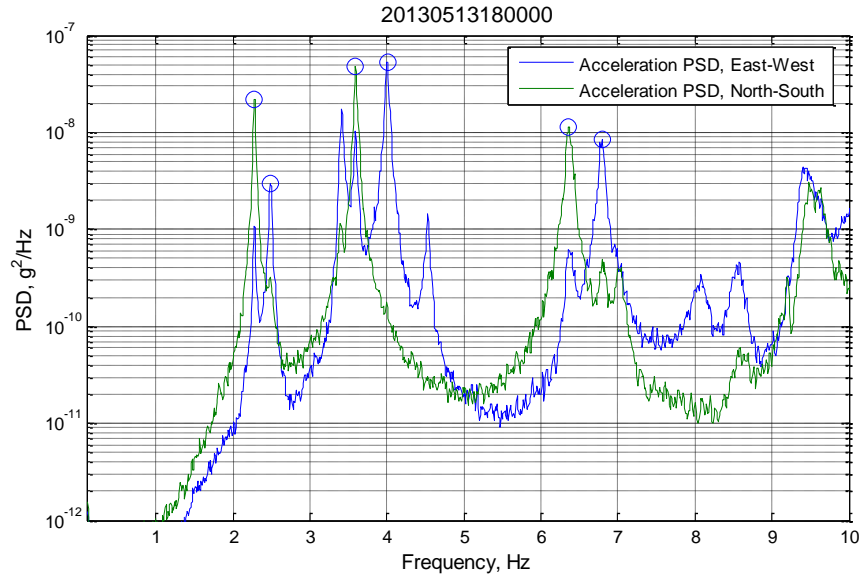


Figure 3.3: Acceleration power spectral density

The PSD signal is complex in the East-West direction due to the coupling between the East and Central Towers. The East-West direction signal peaks at larger frequencies for all three modes, showing that the tower is stiffer in that direction than it is in the North-South direction. Since the Central Tower is approximately symmetrical, this increase in stiffness is likely due to the coupling of the two towers.

The dominant frequencies were identified for each one-hour set of data using the previous methods. The following plots display the shift in frequency relative to the variations in temperature.

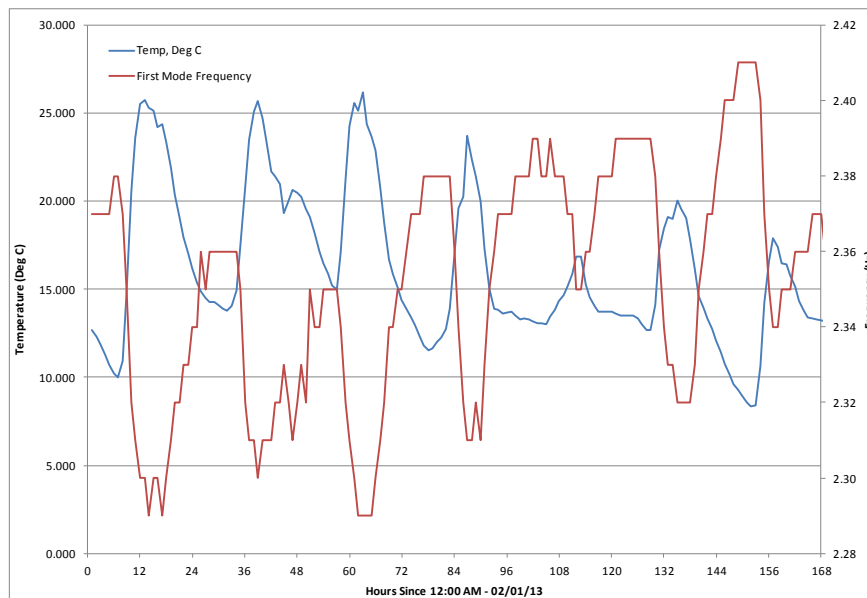
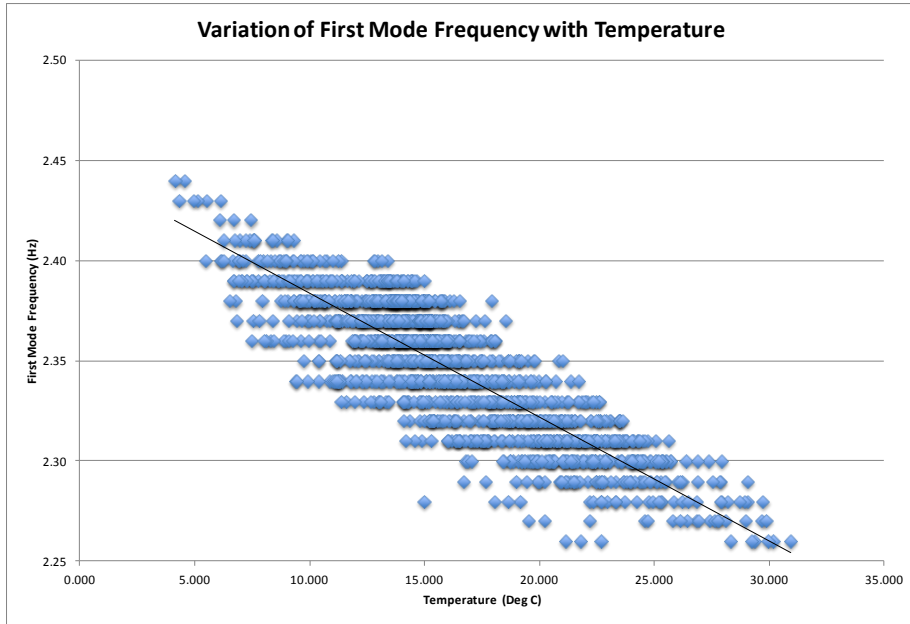
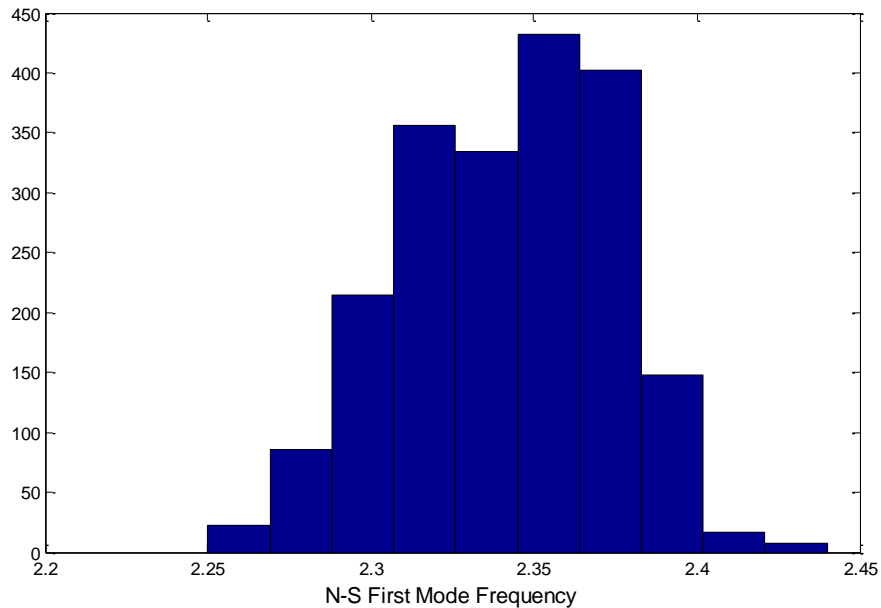


Figure 3.4: Frequency variation with temperature over time

A clear trend can be seen in this figure: As the temperature increases, the stiffness of the tower decreases, causing a drop in first mode frequency. The Central Tower acts as an unrestrained cantilever. As the temperature increases, the structure expands and the material becomes more flexible. It was found that throughout the day, the first mode frequency in the North-South direction could vary by as much as 5%; and over the course of several days, the variation is as high as 8%. The frequency of a structure is proportional to the square root of the stiffness, and inversely proportional to the square root of the mass. Since the mass remains constant, an 8% shift in frequency corresponds to approximately a 15%-shift in stiffness. This same trend can be seen over the course of a few months through the figures below, which show the hourly variation in frequency between January 30th, 2013 and May 12th, 2013.



**Figure 3.5: January - May frequency vs temperature**



**Figure 3.6: Frequency histogram**

This daily shift in frequency has two important effects. The first is that the stiffness and corresponding frequency of a structure will change the amount of shear force experienced during an earthquake. According to the ASCE 7-10's equivalent lateral force procedure, the upper-bound base shear experienced during an earthquake is inversely proportional to the period, and therefore directly proportional to the frequency of the structure. A 5 to 10% increase in frequency can theoretically lead to an increase in the base shear by the same amount.

Another important implication of this shift in frequency is from a structural health-monitoring standpoint: with such a strong correlation between ambient temperature and frequency, a shift in the frequency would be masked by the environmental factors. In order to use any form of vibration based damage detection, the data would need to be first be cleansed of the environmental effects.

### 3.3 Daily Tilt Cycles

Plants will grow toward a light source in order to maximize the amount of energy available for photosynthesis, a behavior known as phototropism. The Central Tower conversely leans away from the sun over the course of the day. This trend is due to differential heating of the side exposed to the sun compared to the shaded, cool side. The elements on the sunny side will expand faster, and to a larger extent. The figure below shows the daily tilt cycles in the N-S and E-W directions.

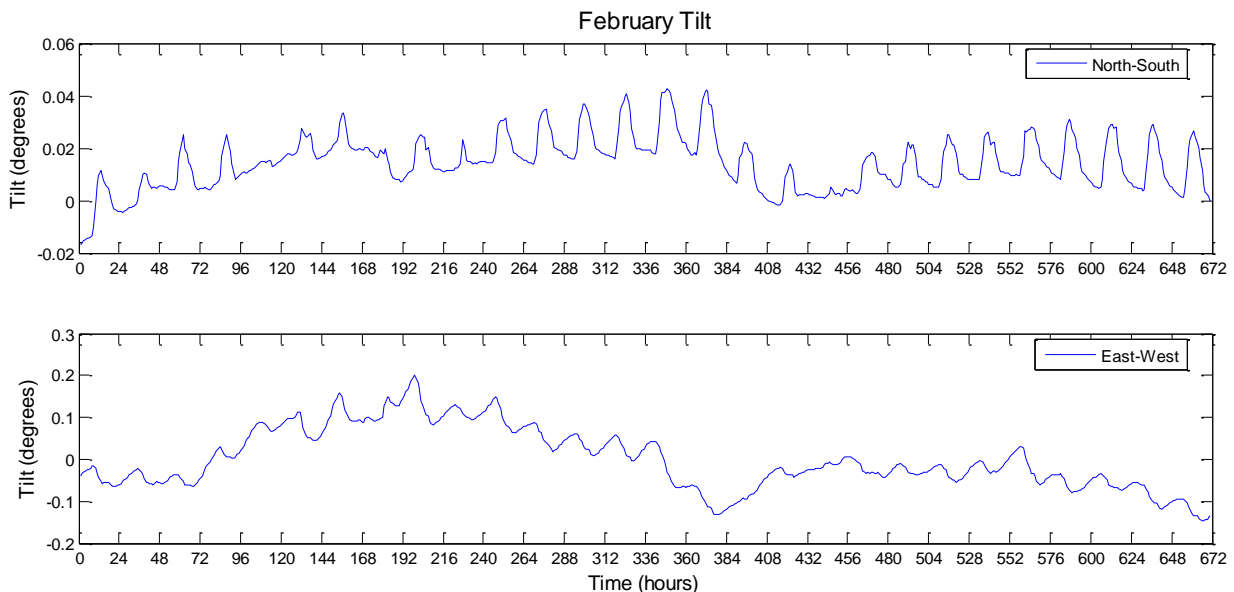


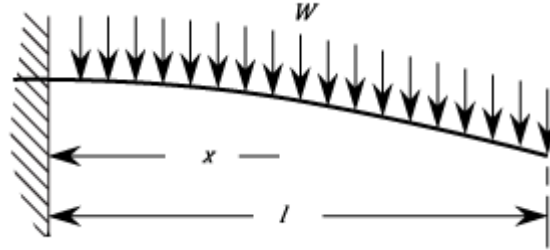
Figure 3.7: February tilt

In the E-W direction, the daily variation is around 0.05 degrees, whereas in the N-S direction the daily variation is smaller—around 0.02 degrees. It is not known at this time why the daily displacement is larger in the E-W direction as compared to the N-S direction. There are a couple of different methods to estimate the tip displacement of the tower given the tilt data. The simplest method is to assume uniform rotation over the height of the tower, in which case the displacement can be found by simple geometry.

$$\Delta_{tip} = H_{tip} \times \tan(\theta_{sensor}) \approx H_{tip} \times \theta_{sensor}$$

Note that  $\theta$  must be in radians to use the small angle approximation of  $\tan(\theta) \approx \theta$ . Using this approximation, the daily tip displacement is around 1 inch in the E-W direction, and 3/8 inches in the N-S direction.

A slightly more advanced method would be to approximate the tower as a uniformly loaded cantilever beam, which would result in the following displacement pattern.



The displacement and rotation at any point along the beam can be calculated using the following two equations where  $x$  is the location along the beam,  $l$  is the total length,  $w$  is the magnitude of the loading,  $E$  is the Young's modulus, and  $I$  is the second-moment of cross-sectional area.

$$\theta(x) = \frac{w}{6EI}(x^3 - l^3) \quad \Delta(x) = \frac{w}{24EI}(x^4 - 4l^3x + 3l^4) \quad \Delta_{tip} = \frac{wl^4}{8EI}$$

The value for rotation is known at the location of the sensor,  $x = 23$  ft. Plugging in this value along with a total length of  $l = 96.75$  feet, and then taking the ratio, allows the tip displacement to be estimated as follows:

$$\Delta_{tip} = \theta_{sensor} \times \frac{6(96.75^4)}{8(23^3 - 96.75^3)} = -73.55 * \theta_{sensor}$$

The above equation is valid when  $\theta$  is in radians, and the resulting displacement is in feet. This method estimates the daily displacement at -0.77 inches in the E-W direction and 0.31 inches in the N-S direction. Note that  $E$  and  $I$  were assumed to be constant over the length of the tower, and their values cancelled out when finding the relationship between rotation and displacement. It is likely that the tip displacement is even larger because the stiffness of the tower decreases along its height as the columns all move closer to the center. Results from a computer model can be used to update this approximation.

In both directions, there is a noticeable long-period drift to the data. These trends may be a function of electronic drift or might reflect real behavior. The values tend to return to zero however, which suggests that it is an actual behavior of the towers. One possible explanation is that during abnormally hot days, the tower tilts to a more extreme angle and during the night doesn't fully return to its initial position before the next daily cycle. Figure 3.8 displays the average daily temperature along with the peak daily tilt for the month of February.

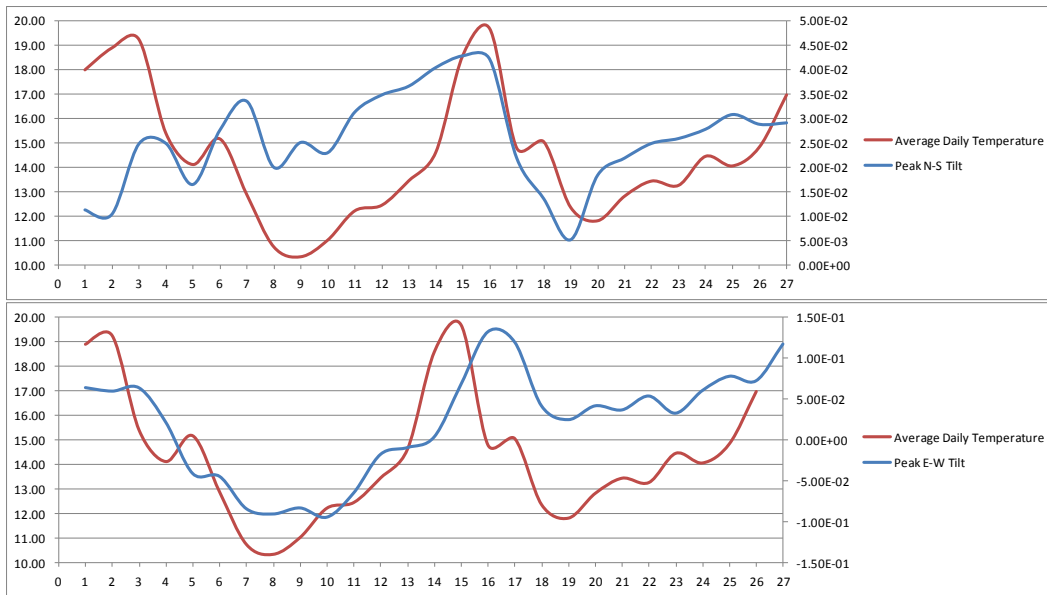


Figure 3.8: Average daily temperature versus peak daily tilt

The above plots of temperature and tilt seem to follow the same pattern, suggesting that this theory has some credibility. The relationship is stronger in the E-W direction than it is in the N-S direction.

In order to better visualize the daily motion without the long-term effects, the data was filtered using a fifth-order Butterworth band-pass filter, which is available in Matlab's signal processing toolbox. The low-pass frequency was set at  $1/30$  [1/hr] and the high-pass frequency was set at  $1/18$  [1/hr]. The filtered data is shown below.

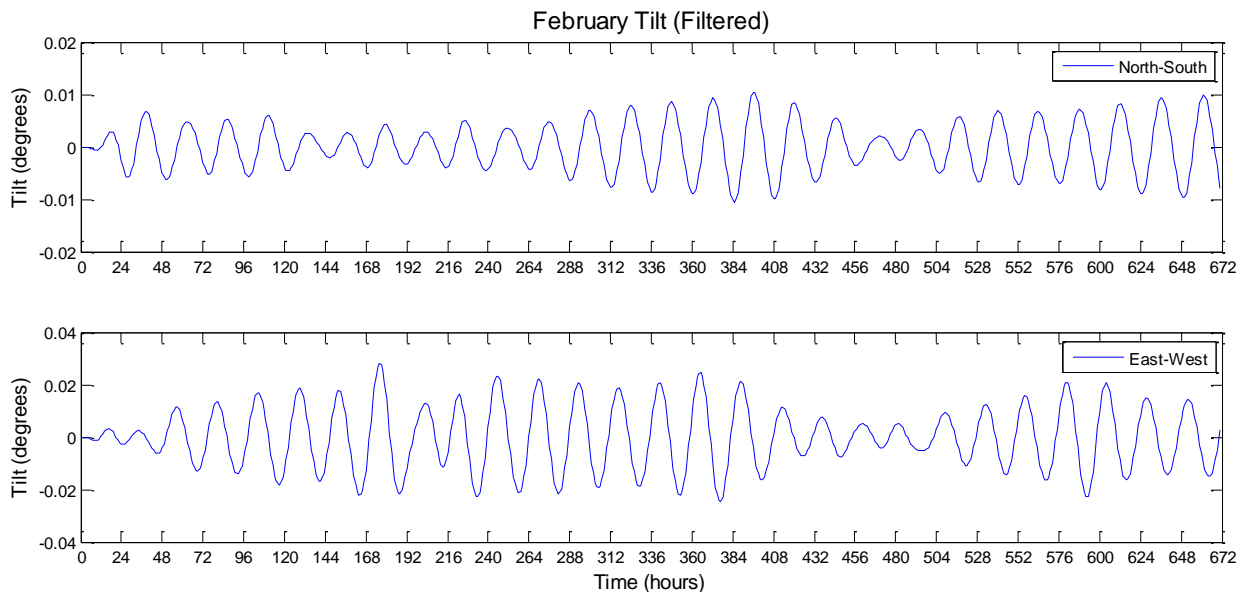
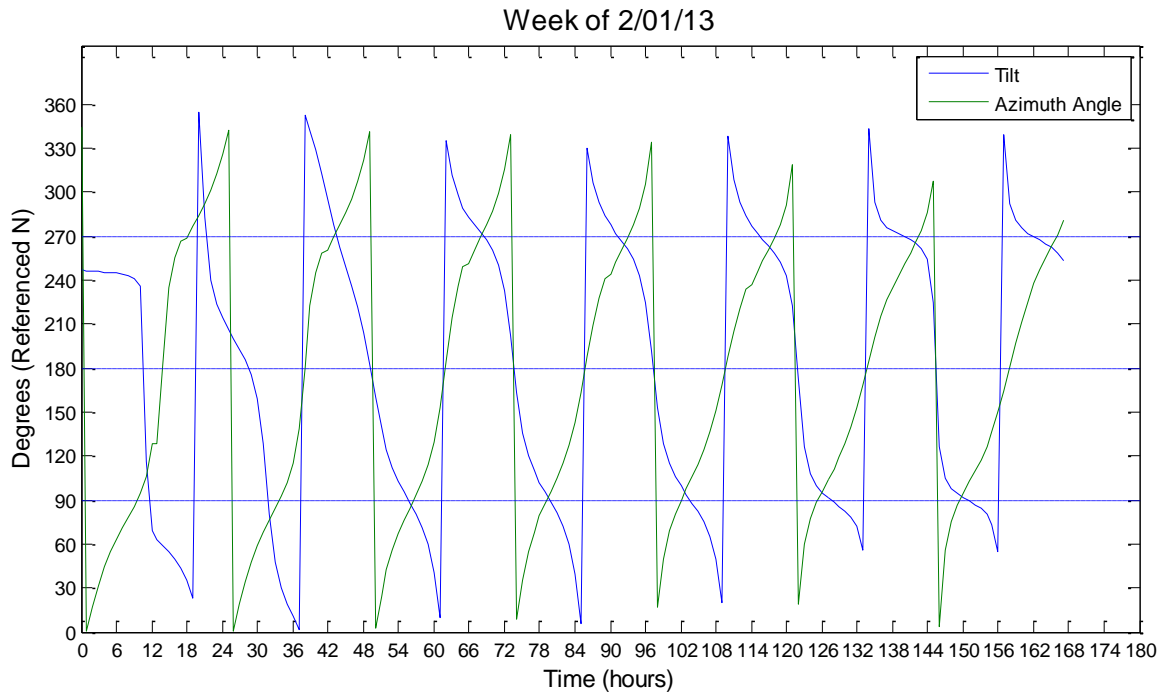


Figure 3.9: Band-pass filtered February tilt

It was hypothesized that the tilting behavior of the structure is governed by the direction of incoming sunlight. The position of the sun was calculated knowing the site coordinates (longitude, latitude, and elevation) and time of day. The position is commonly reported using an

azimuth angle (position in the horizontal plan relative to North) and an elevation angle (position in the vertical plane relative to the ground surface). Plotting the azimuth angle versus the resultant tilt of the structure allows the hypothesis to be tested.



**Figure 3.10: Week of 2/01/13 tilt vs azimuth angle**

The tower motion does in fact correlate well with the azimuth angle. There are three times of day to note in the plot. At sunrise (~7 am), both the tilt and azimuth are approximately due East. The same behavior is seen at sunset (~8 pm) when the tilt and azimuth are in the West. In the middle of the day however, the sun is located to the South, and the tower is directly opposite leaning toward the North. The daily cycle is then, the tower and sun “meet” at sunrise in the East. The tower moves counter clockwise toward the North as the sun rotates in a clockwise direction toward the South.. At noon, the tower is at its most northern point whereas the sun is at its most southern point. They continue to move until the sun and tower both reach the West. At this point the sun sets, and the tower continues its counterclockwise rotation toward the East, where it is again met by the sun the following day. This circular behavior is clearly seen in the next set of plots, which show the track of the tower throughout the month of February, and the location of the tower at the previously noted three times of the day. Note that the sunrise and sunset times are approximated in these figures. The magnitude of displacement is based off the uniform rotation approximation.

Animation videos of this measured behavior have been created to better visualize the phenomenon. These videos have been transmitted to LACMA and other interested parties.

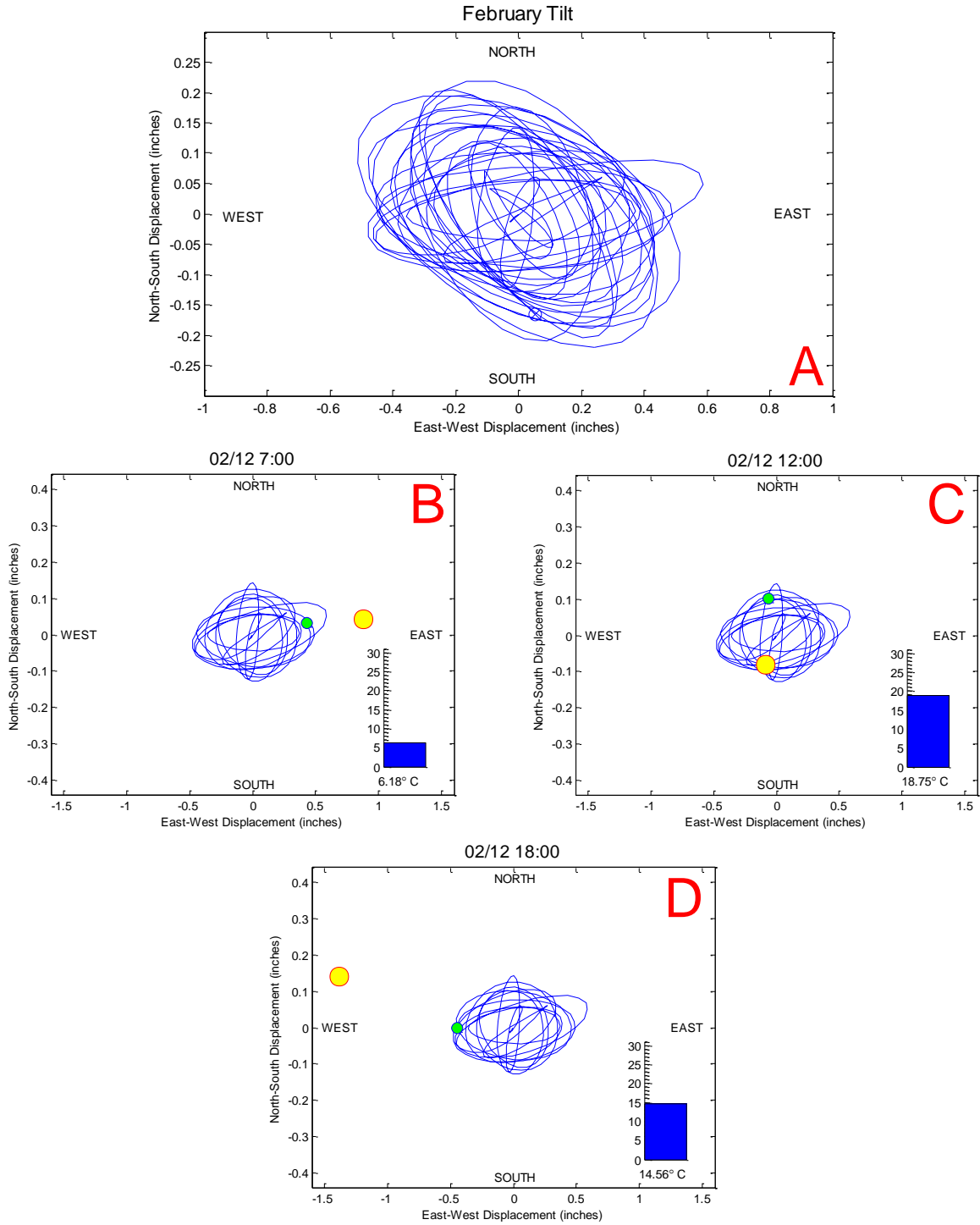


**Figure 3.11: Daily tilt cycles (A) month of February (B) sunrise (C) noon (D) sunset**

### 3.4 Earthquake and Wind Response

#### 3.4.1 Earthquakes

The towers have stood the test of time against frequent small, and a few large-amplitude earthquakes and windstorms. The following table summarizes a few major southern California earthquakes of the past century, and their distance to the towers.

Table 3.1. Notable Earthquakes in Proximity of the Towers

Name	Year	Mag.	Epicenter Latitude	Epicenter Long.	Distance (km)
Long Beach	1933	6.4	33.63	-117.99	25.8
Kern	1952	7.5	35.00	-119.01	137.5
Sylmar	1971	6.6	34.24	-118.24	20.8
Whittier Narrows	1987	5.9	34.06	-118.08	20.1
Sierra Madre	1991	5.8	34.26	-118.00	42.1
Landers	1992	7.3	34.13	-116.26	114.3
Big Bear	1992	6.5	34.20	-116.82	84.5
Northridge	1994	6.7	34.12	-118.32	13.33
Hector Mine	1999	7.1	34.59	-116.27	121.3
Inglewood	2009	4.7	33.94	-118.35	6.3
Pico Rivera	2010	4.4	33.99	-118.08	9.8

Note that the 1933 Long Beach Earthquake ruptured the Newport-Inglewood Fault, with surface rupture observed within 2 miles of the Watts Towers. The towers were in the early stage of construction then, and damage is not well-documented. But shaking would have been very strong during that earthquake, as it would be for future earthquakes on the Newport-Inglewood Fault.

Due to the high seismicity in this area, it was hoped that several earthquakes would occur during the duration of the monitoring. Unfortunately, as of now, only a few small earthquakes have been recorded. The most notable was the March 11 Anza Earthquake, which was an M4.7 earthquake with an epicenter approximately 172 Km from the towers. The acceleration and tilt responses to this earthquake are shown in the figure below.

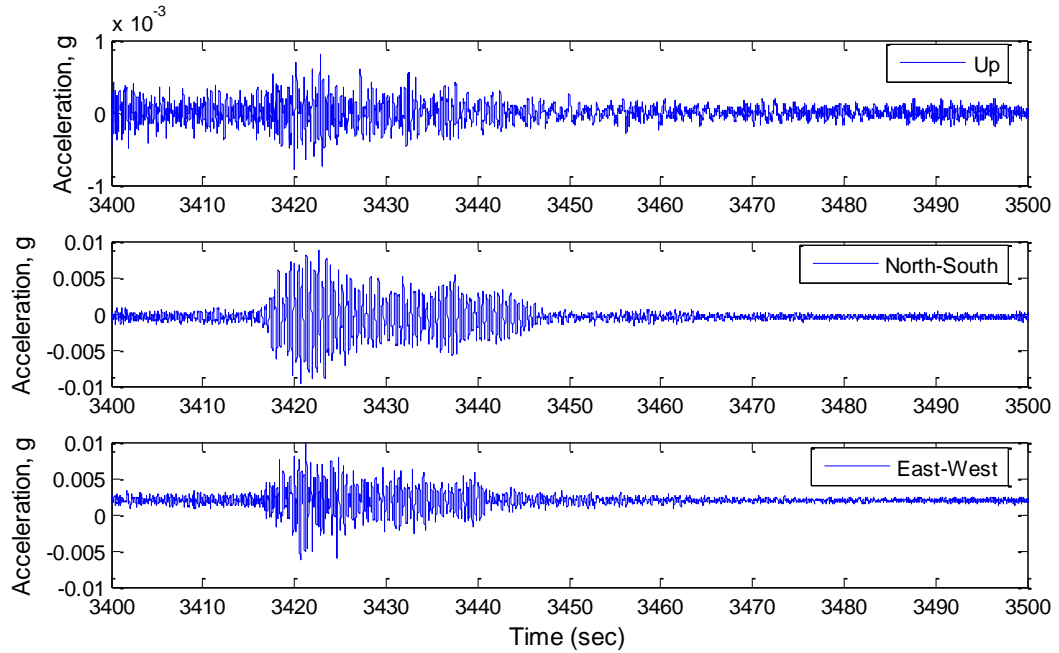


Figure 3.12: Acceleration response to the March 11, 2013 Anza Earthquake

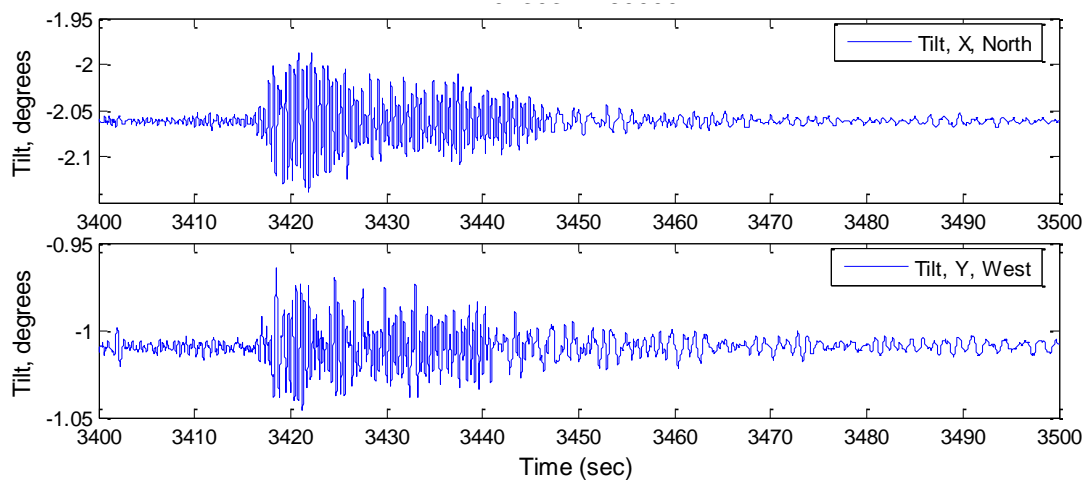
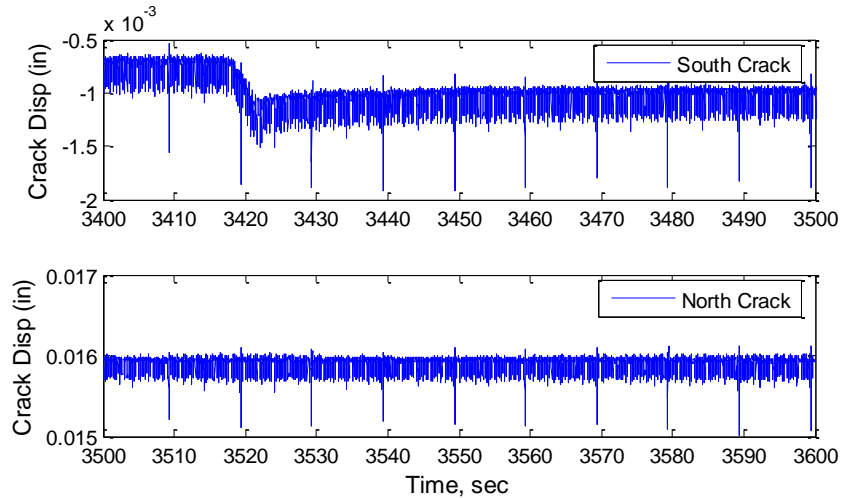


Figure 3.13: Tilt response to the to the March 11, 2013 Anza Earthquake

Both the N-S and E-W components of acceleration reach approximately  $0.01g$ , while the vertical component is much smaller and only reaches a maximum of  $0.001g$ . This vibration is still very low, but is about 10 times larger than the ambient vibrations. The earthquake clearly registered on the tilt sensor as well, with peak-to-peak movement of about 0.1 degrees. Using the previously derived cantilever approximation, this results in around 1.5 inches of displacement at the tip of the central tower.



**Figure 3.14: Crack response to the to the March 11, 2013 Anza Earthquake**

The figure above displays the north and south crack displacements during the earthquake. In the south crack, there is a noticeable movement around 3415 seconds, which corresponds almost exactly with the first pulse of the earthquake. Unfortunately, this small-amplitude data is from the period in which the displacement sensor had a noisy power supply that reduces the precision of the measurements.

It has been seismically very quiet in Los Angeles so far in 2013. One target of our continued data collection at WattsTowers is to capture larger-amplitude earthquake shaking with improved precision..

### 3.4.2 Wind

The towers are surrounded in every direction by low-rise (one- and two-story) residential construction. This means that there is no significant object that can break the winds, and thus, the 100-foot tall Towers nominally face the full force of the Santa Ana winds. In April 2013, a windstorm hit the towers with speeds peaking over 30 mph at the height of the wind sensor, which is approximately 15 feet.

The following plots show the wind speed, acceleration, tilt, and crack response during a four-minute period of high wind gusts.

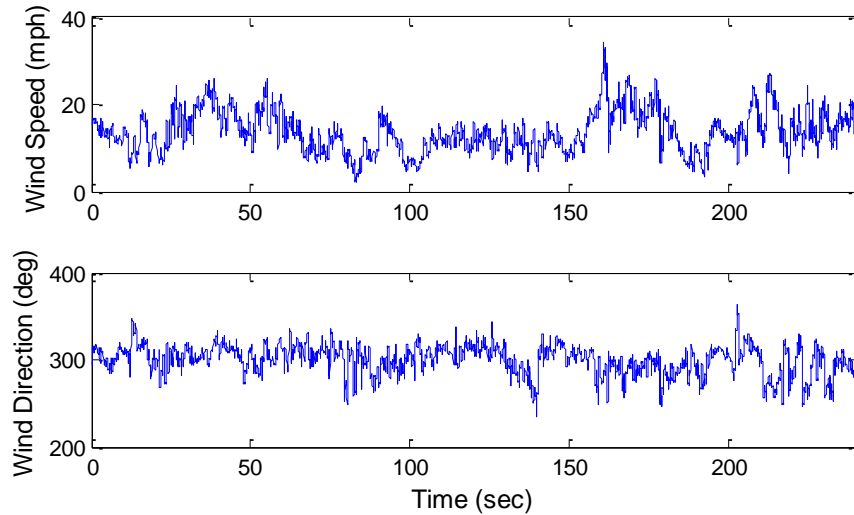


Figure 3.15: Wind speed and direction

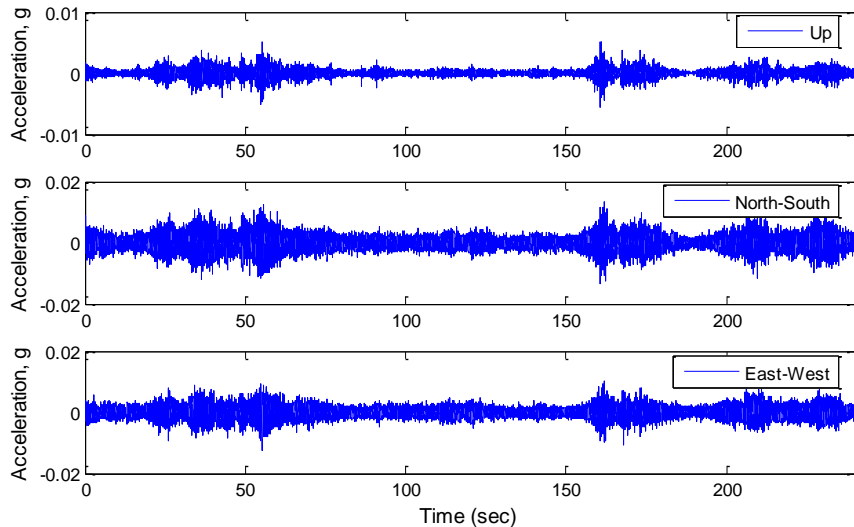


Figure 3.16: Wind storm acceleration response

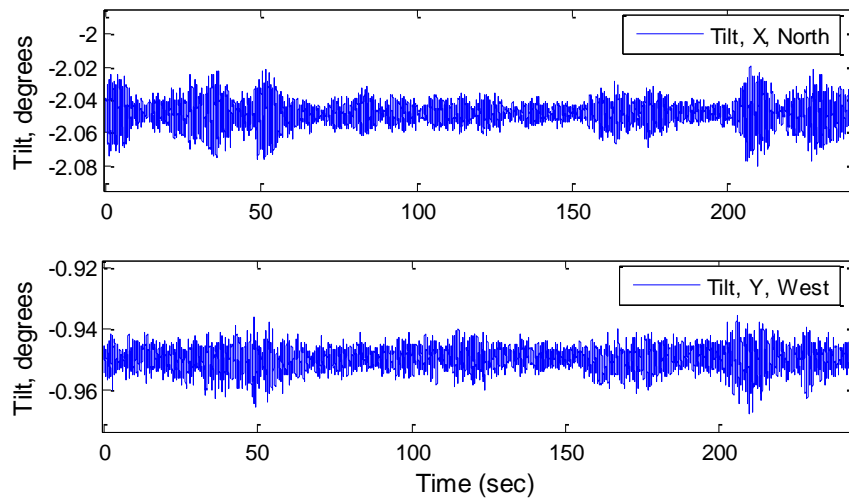


Figure 3.17: Wind storm tilt response

The primary wind direction is Northwest, with the strongest acceleration response in the N-S direction. The peak accelerations in the N-S and E-W directions are  $0.016g$  and  $0.014g$ . The peak-to-peak tilt magnitudes are 0.06 degrees and 0.02 degrees in the N-S and E-W directions respectively, which yield approximate displacements of 0.92 inches and 0.31 inches. When compared to the earthquake response, the windstorm caused larger accelerations, but the overall displacement was smaller.

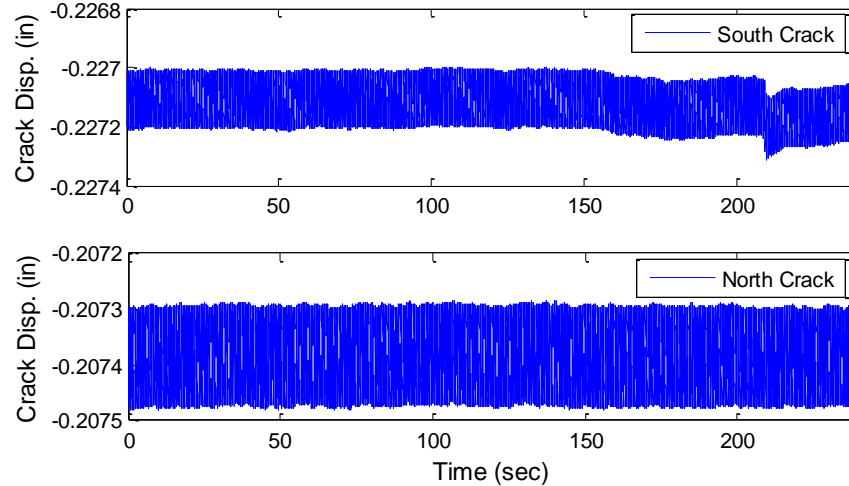


Figure 3.18: Wind storm crack response

Looking at the above plots, other than a small shift in the south crack, the wind doesn't appear to have any dynamic affect on the crack movement.

### 3.5 Crack Displacement

The end goal of this study is a preservation plan that can help to repair existing cracks and ideally prevent new cracks from forming. In order to accomplish this, it's necessary to understand how the cracks are behaving. Two cracks were selected along the base of the Central Tower's exterior columns as shown in the diagram below.

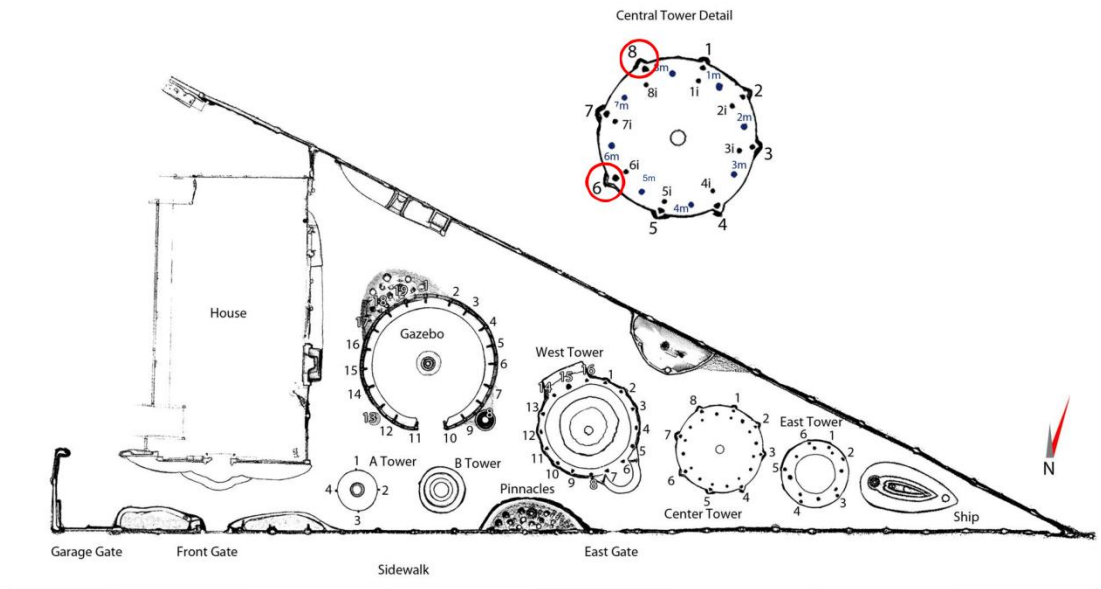


Figure 3.19: Crack displacement sensor locations

The Central Tower's columns were also instrumented by the LACMA team with two different types of sensors. On column 8, LACMA placed a TML PI-2 displacement transducer, which works by attaching a combination of strain gauges across an arch-shaped spring plate. Column 6 was instrumented with another PI-2 sensor, as well as a UB-5A displacement transducer. Mounting of the UB-5A transducer requires cutting into the column around the crack, whereas the Pi-2 is surface mounted with epoxy.

The following plots show the north and south crack displacement as recorded by both the UCLA and LACMA systems.

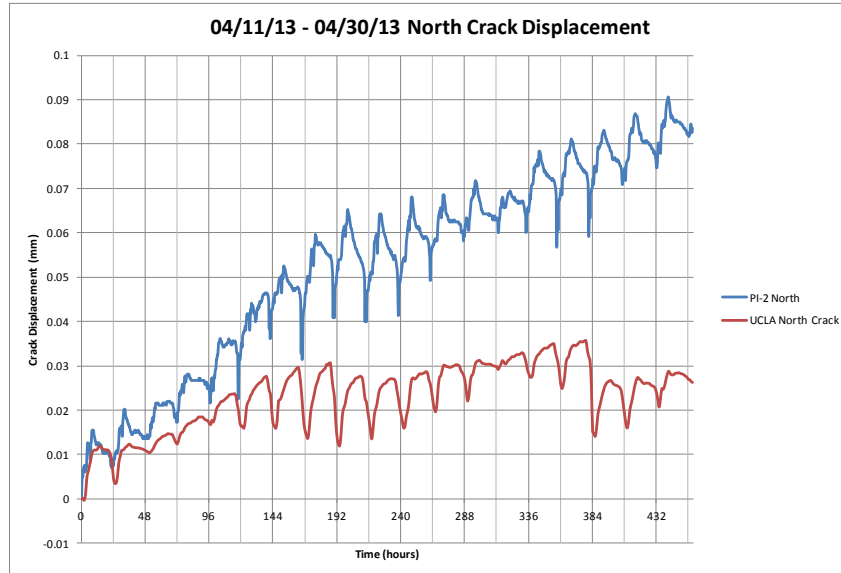


Figure 3.20: LACMA vs UCLA north crack displacement

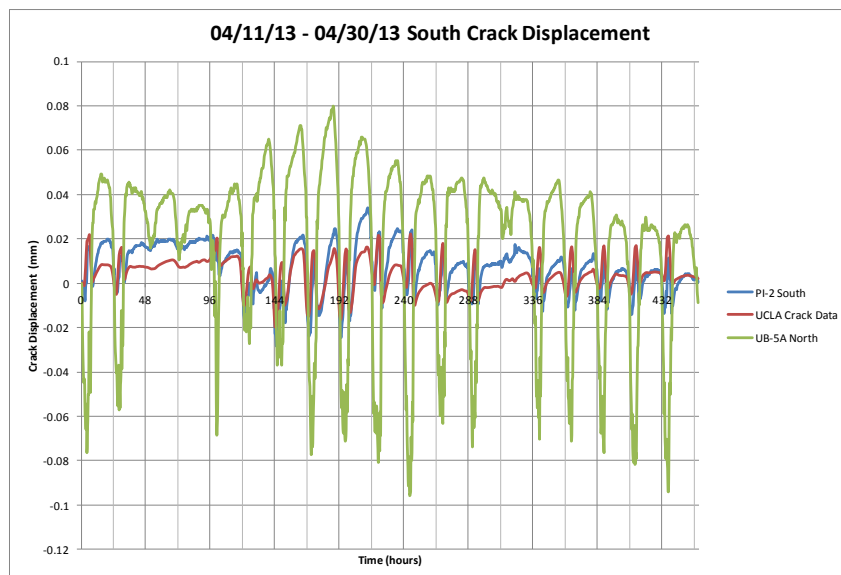


Figure 3.21: LACMA vs UCLA south crack displacement

The first thing to note in Figure 3.21 is that the north crack appears to be drifting off of its baseline. Since the same behavior is observed by independent sensors, it is possible that this suggests a gradual opening of the crack and not an electronic drift in the signal. The south crack, on the other hand, displays a more widely variable behavior; yet over time, it tends to remain around a set baseline.

Comparing the two systems, it is noted that the LACMA Pi-2 sensors seem to correlate well with the UCLA sensors. Although the magnitudes are slightly off for the south crack and the amount of drift is exaggerated in the north crack, the overall behavior and daily peak values are very similar. The LACMA UB-5A sensor is recording much larger displacements, which likely are not correct. It was originally hypothesized that the UB-5A was the more accurate sensor, but

these results contradict those findings, and if the tower is to be further instrumented, it is recommended to use the Pi-2 sensors.

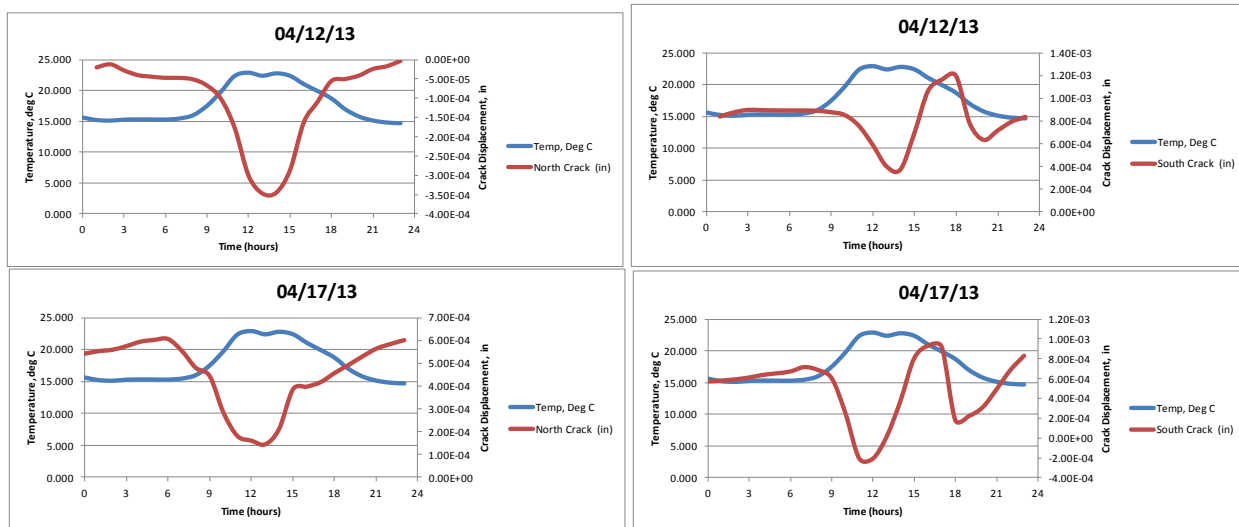


Figure 3.22: North and south crack displacement for 4/12 and 4/17

On a daily basis, the cracks display remarkably consistent, albeit distinct, behaviors. The north crack follows an inverse relationship with temperature. As the temperature increases the crack tends to close. This is likely due to the concrete cover expanding. If the steel reinforcement dominated the daily crack behavior, then the crack would tend to open as the temperature increases. The south crack, on the other hand, has a bimodal shape that bottoms out around noon each day, before opening back up until around 4-6pm. At sunset, the crack starts to close again. The daily displacement for the north crack is around 0.0004 inches, whereas the south crack is more active with a larger daily displacement of 0.001.

Throughout the day, the north crack remains in the shade, while the south crack is exposed to direct sunlight. We hypothesized that this direct exposure to sunlight may explain not only the difference in magnitude between the two cracks, but also the difference in their behaviors. Therefore on a day where there is very little sunlight the two cracks should behave similarly. As an initial test of this hypothesis, the solar radiation data from the LACMA weather station was examined. It was theorized that a day of low solar radiation would correspond with a cloudy, overcast day, and the effect of direct sunlight would be smaller.

The following plot shows the peak daily solar radiation, and temperature for the month of June 2013. June was examined in the hopes of finding the typical California “June Gloom” days. Four days were selected: two days with low solar radiation, and two days with high solar radiation. Through comparisons with the temperature data, these days also correspond fairly well with high and low temperature days.

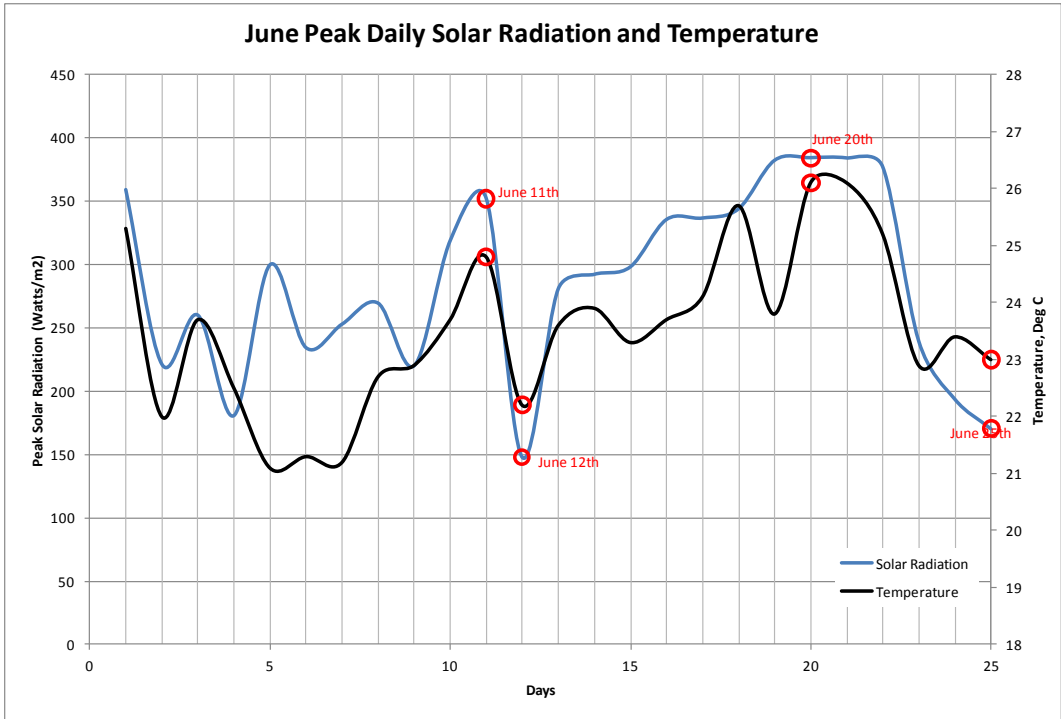


Figure 3.23: Peak Daily Solar Radiation

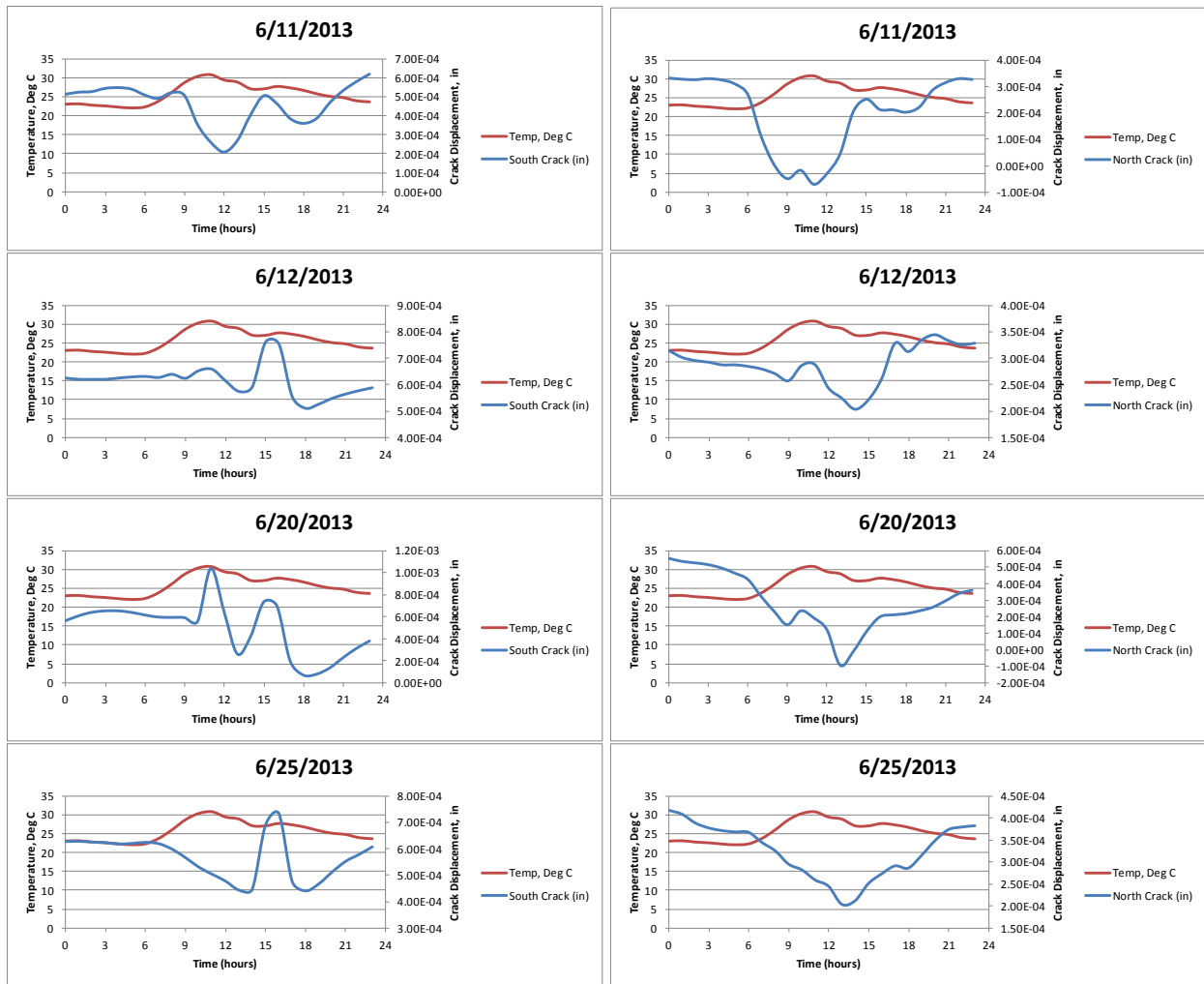


Figure 3.24: Selected daily crack displacement for high and low solar radiation days

Other than a few small anomalies, the north crack follows the same pattern. On the two high radiation/temperature days, the north crack opened and closed a total of 0.0004 and 0.0006 inches. On the low radiation/temperature days, the displacements were much smaller, 0.00014 and 0.0002 inches.

The south crack follows the same pattern on three of the four days; but on June 20th an abnormal opening is seen around 10 am. Other than that, they all follow the same pattern of reaching a minimum around 12-2 pm, and then a maximum around 3-4 pm, and finally reaching a second minimum point around 6pm. The total displacement on the hot days was 0.00041 inches and 0.00097 inches, whereas for the colder days, it was 0.00025 and 0.00029 inches for both days.

These data show that the overall magnitude of the crack movement is dependent on the temperature or radiation, but a shift in behavior wasn't seen for the low radiation days. Even on low-radiation/overcast days, the south crack will receive some direct sunlight, which may still

affect its behavior. In order to better test the effects of direct sunlight, a shade experiment was devised that involved covering the south-side crack with an 8'x12' double layered canvas tarp as shown in the photographs below. The crack sensor is circled in the right picture.



Figure 3.25: Shade experiment setup

The shade was setup in the afternoon of July 29<sup>th</sup>, and left until the afternoon of July 31<sup>st</sup>. The plot below shows the crack displacement from July 30<sup>th</sup>, the day in which the crack was covered from beginning to end.

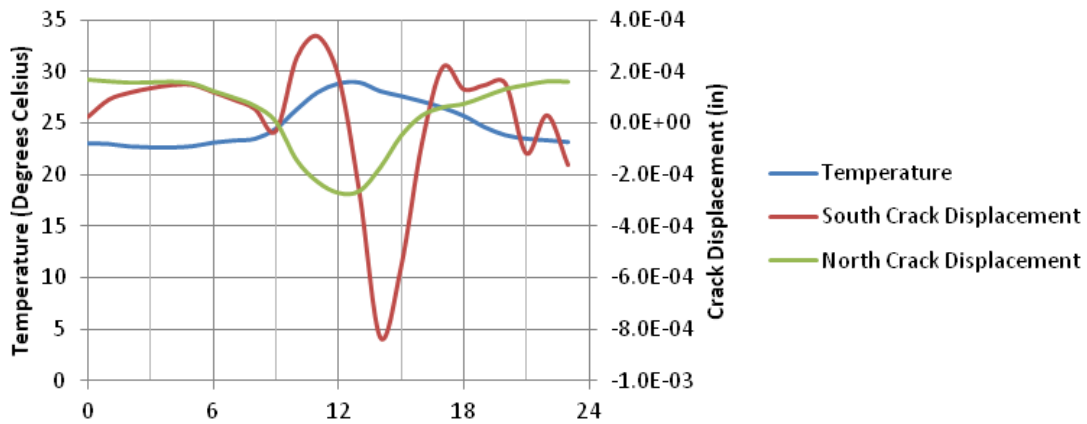


Figure 3.26: Shade experiment crack displacement

If the hypothesis were entirely correct, the south crack's shape should be similar to that of the north crack. While this wasn't the case, the south crack still displayed a unique behavior that wasn't observed on previous days. The initial opening around 10 am is similar to what was seen on June 20<sup>th</sup>, but after reaching a minimum at 2 pm the crack reopens until 5 pm at which point it starts to oscillate around its equilibrium location. On a typical day, another closing cycle would have been observed.

With only one full day of data to investigate, and a shape that is still highly irregular, it is not possible to conclude with certainty whether (or not) the direct sunlight exposure is the cause of the south crack's behavior. The shift in shape, nonetheless, lends credibility to the theory. A

better test of local heating effects could involve a larger, more reflective tarp that is attached higher up on the tower. It may also be possible to provide a small AC unit, or other method of controlling the local environment. Another option is to wait until the next rain storm and examine the behavior from such a day. During a rainy day, there will be extensive cloud cover, which will block sunlight. The rain will also help to cool the structure, minimizing any differential heating between the two sides. Future data collection will provide answers to this question.

### 3.6 East to Center Tower Coupled Motion

On July 30<sup>th</sup> all three towers were instrumented with a total of five triaxial accelerometers as shown in the figure below.

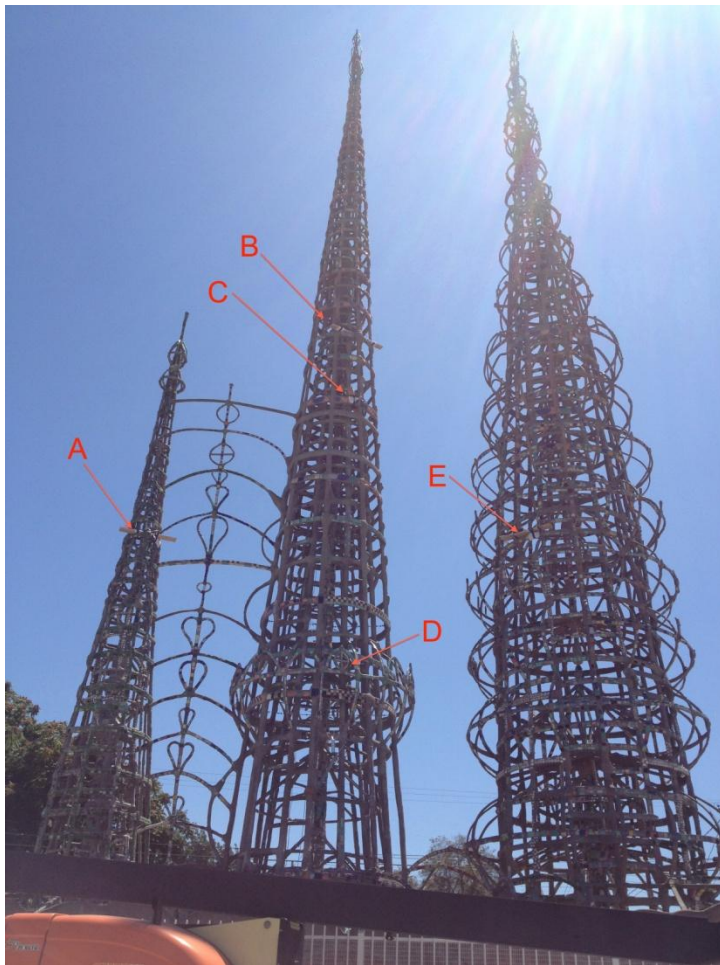


Figure 3.27: Coupled motion sensor arrangement

Table 3.2. Sensor Locations

Label	Tower	Height (feet)
A	East	32.72
B	Center	52.16
C	Center	45.14
D	Center	22.81
E	West	33.58

A total of 12 beams span the gap between the East and Center Towers, starting at a height of 11 feet and ending near the top of the East Tower at just under 45 feet. It was hypothesized that these beams would lead to a strong coupling of motion between the two towers, with the taller, heavier Center Tower driving the motion of the smaller East Tower. There are also a few smaller overhead arches that connect the Center and West Towers around the 8-10 foot elevation. Since these arches are near the base of the towers, where the structures are very stiff, it is unlikely that they will lead to significantly coupled motions. The two main goals of this sensor arrangement were to quantify the amount of coupling, as well as to estimate the stiffness of the other towers by finding their fundamental frequencies. To accomplish the first goal, one of the exterior columns along the base of the Center Tower was shaken by hand, first in the N-S direction and then in the E-W direction.

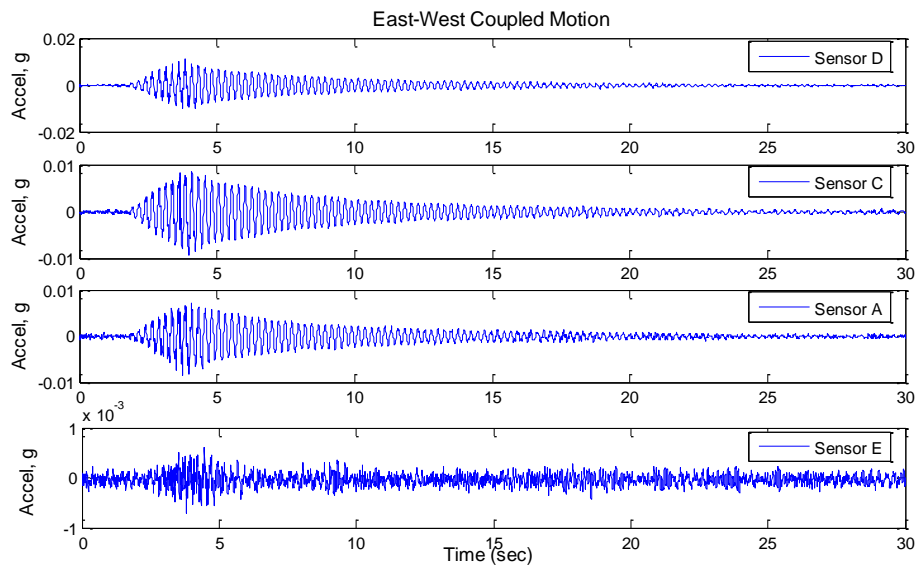


Figure 3.28: East-West acceleration transfer between towers

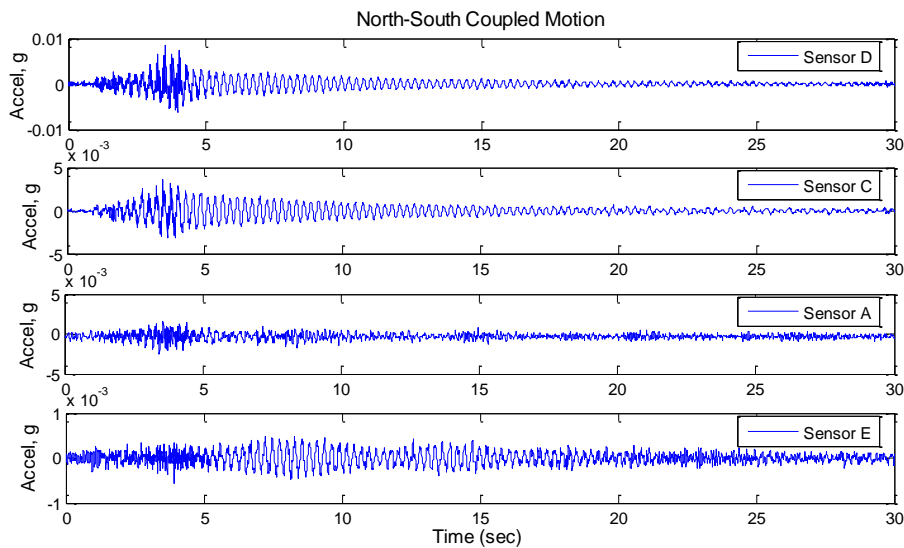


Figure 3.29: North-South acceleration transfer between towers

Recall that sensors D and C were the two lowest accelerometers on the Center Tower, sensor A is on the East Tower, and sensor E is on the West Tower. In the East-West direction the coupling is immediately clear between the East and Center Tower. The peak acceleration for the two sensors on the Center Tower was 0.011 and 0.0093. The peak acceleration on the east tower is 0.0086g, a remarkably high 77% of the acceleration recorded at sensor D. This proves the hypothesis of the two towers (Center and East) being significantly coupled. However, when looking at the response of the West Tower, only a small increase above the ambient vibration is seen, and the peak acceleration is only 6% of that on the Center Tower. This suggests an almost negligible coupling between the West and the Center Towers.

In the North-South direction the coupling is also negligible. Any coupling in this direction would be dependent on the flexural stiffness of the connecting beams. Since these elements are long and fairly slender, their flexural stiffnesses are very low.

The `pwelch` function was again used in Matlab to obtain the averaged power spectral density of the East and West Tower acceleration signals, and to estimate the first three fundamental frequencies. The resulting plots are shown below. The first three fundamental frequencies for each tower are summarized in Table 3.3.

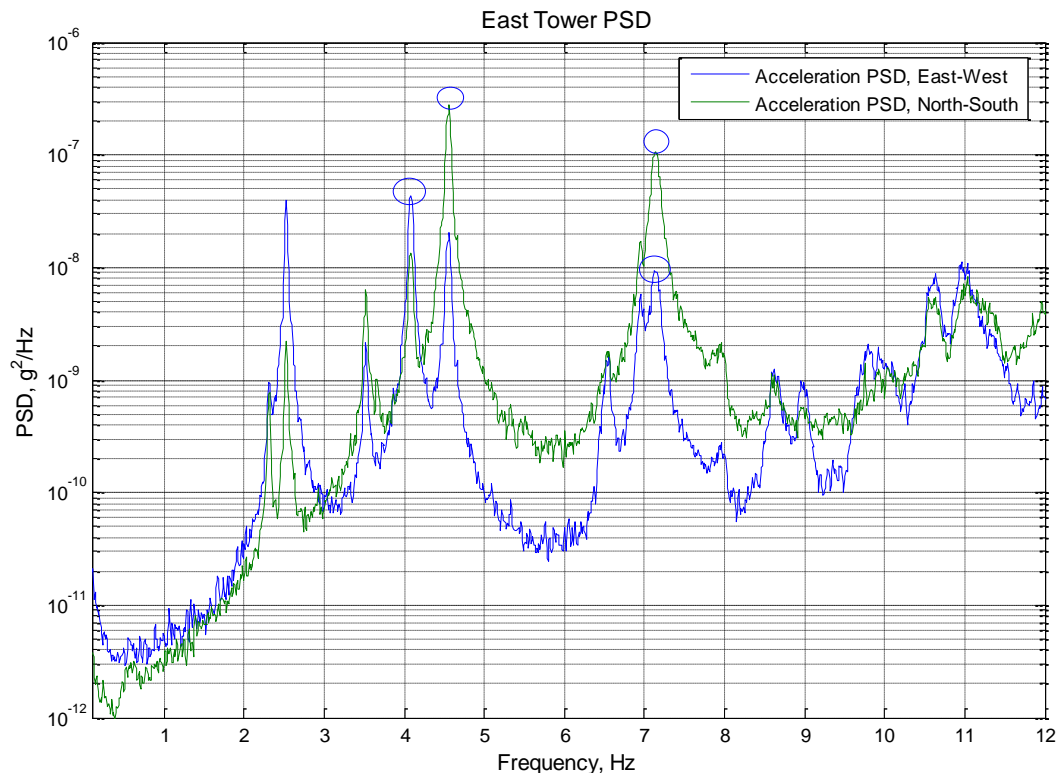


Figure 3.30: East Tower power spectral density

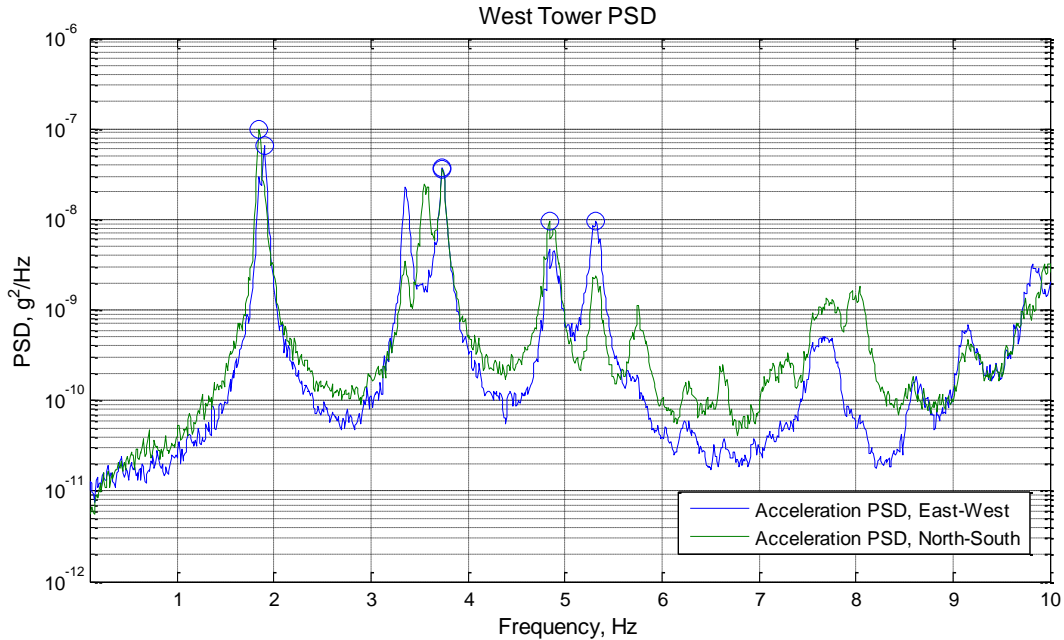


Figure 3.31: West Tower power spectral density

Table 3.3. Fundamental frequencies

	North-South Frequency (Hz)			East-West Frequency (Hz)		
	$f_1$	$f_2$	$f_3$	$f_1$	$f_2$	$f_3$
East Tower	4.56	7.14	-	4.09	7.13	-
Center Tower	2.34	3.73	6.66	2.56	4.14	7.11
West Tower	1.85	3.74	4.84	1.9	3.73	5.32

The East Tower has the highest first and second mode frequencies. This is an expected result, because it is the shortest tower and therefore the least flexible. The East Tower spectrum shows two earlier peaks below 4 Hz, but these are around the same frequency as the first two modes of the Central Tower, and are likely caused by the coupling action.

The West Tower has the lowest frequencies. The West and Central towers are similar in height and weight, but the West Tower has a more open construction with only 16 columns arranged in one layer, and fewer bands and spokes, resulting in a reduced stiffness. The West Tower was the last one built (Goldstone, 1997, p. 50), and it's possible that the experience gained from building the first two towers helped to give Rodia the confidence to build a more open, less redundant structure. Note that since the West Tower is uncoupled from the other two, its spectrum is almost perfectly symmetrical between the E-W and N-S directions.

A further benefit of the manual excitation test of the Center Tower has been regarding the estimation of structural damping. Note that a very clean exponentially decaying signal is seen in the acceleration measurements during this test. Elastic vibration theory states that a single degree-of-freedom structure will undergo free vibration decay according to the following formula (Chopra, 2007):

$$u(t) = e^{-\xi\omega t} \left[ u_0 \cos(\omega_d t) + \frac{\dot{u}_0 + \xi\omega u_0}{\omega_d} \sin(\omega_d t) \right]$$

where  $\omega$  and  $\omega_d$  are the undamped and damped frequencies,  $u_0$  and  $\dot{u}_0$  denote the initial displacement and initial velocity, and  $\xi$  is the damping ratio, expressed as a percentage of critical damping. When the damping ratio isn't known, the so-called log-decrement approach can be used to estimate its value, using the equation

$$\xi = \frac{1}{2\pi} \ln \frac{u_n}{u_{n+1}}$$

where  $u_n$  is the peak displacement for one cycle, and  $u_{n+1}$  is the displacement at the next peak. A segment of the acceleration signal from Sensor D was used to estimate the damping in both directions.

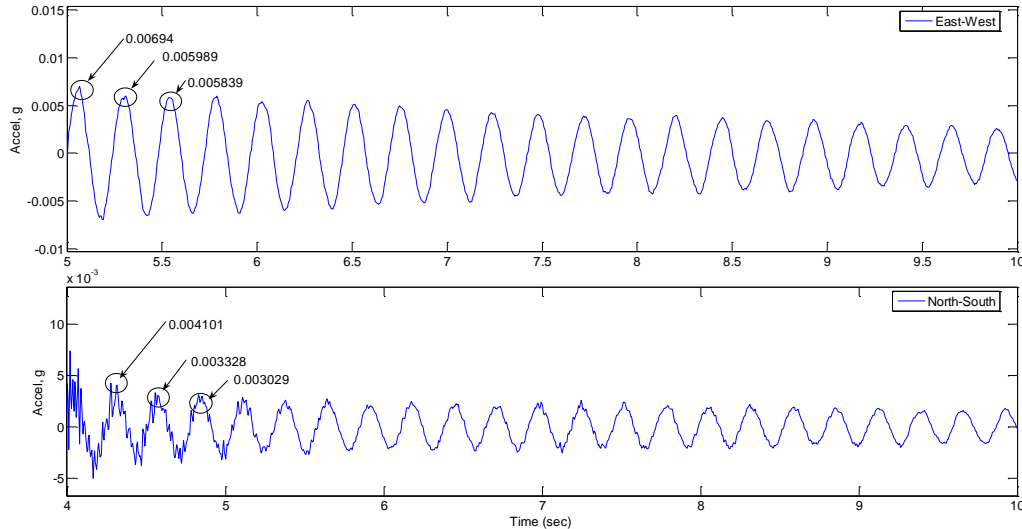


Figure 3.32: Log decrement damping approximation

East-West:

$$\xi = \frac{1}{2\pi} \ln \frac{0.00694}{0.00599} = 2.3\%$$

$$\xi = \frac{1}{2\pi} \ln \frac{0.00599}{0.00584} = 0.4\%$$

North-South

$$\xi = \frac{1}{2\pi} \ln \frac{0.00410}{0.00333} = 3.5\%$$

$$\xi = \frac{1}{2\pi} \ln \frac{0.00333}{0.00303} = 1.5\%$$

Per this approximate method, the damping appears to be in the 1-4% range. Chopra (2007) recommends damping values between 2% and 5% for reinforced concrete, depending on the

amount of reinforcement and cracking. The damping values for the Towers fall within the expected range.

## 4 Computer Modeling

The results of the environmental and vibration monitoring of the Central Tower has provided a wealth of data on how temperature affects the frequencies, tilt, and crack displacements. The data can only tell part of the story, however. A calibrated computer model can be used to study the stress distribution under thermal loading, and possibly explain the initial cause and behavior of some of the cracks. The model can also be used to approximate the behavior during windstorms and earthquakes. While the initial model will only include the Central Tower, it can be expanded at a later date to include the other towers as well, if it is deemed necessary.

In order to develop a model, it was first necessary to define the geometry. A laser scan of the Watts Towers site was completed in October 2011 by GBG USA, (GBG USA). The results of this scan were used to estimate the cross-sectional areas, lengths, and connectivities of the elements that make up the structure.

### 4.1 Lidar Scan

LIDAR is an acronym that stands for light detection and ranging. It works by having a transmitter send out a laser beam, or other light source, and then by recording the time it takes for the signal to return. By rotating the head of the transmitter by very small angles in the horizontal plane, while having a mirror rotating vertically and redirecting the beam, LIDAR is able to quickly measure the distance to a point in 3D space with very high accuracy (National Oceanic and Atmospheric Administration). By moving the transmitter to several different locations around a site, it's possible to capture the geometry from every angle.

The resulting output from a LIDAR scan is known as a "data cloud," which is simply a collection of points that include a 3D location in space, as well as an intensity value that allows the visualizations of textures and colors in the scanned image. The data points are typically very close to each other, resulting in an extremely large amount of data even for a relatively small site. The Watts Towers scan, for example, has yielded over 295 million data points. The following figure displays the completed scan.

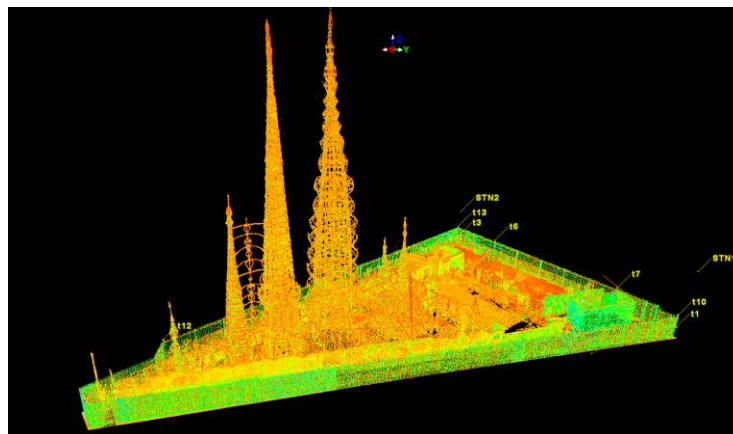


Figure 4.1: LIDAR scan of the Watts Towers site

## 4.2 Defining Model Geometry

The Towers are made of a few typical types of members. For the case of developing the model, the same naming convention was used here that was used in the Ehrenkrantz Preservation Plan (Ehrenkrantz, 1983).

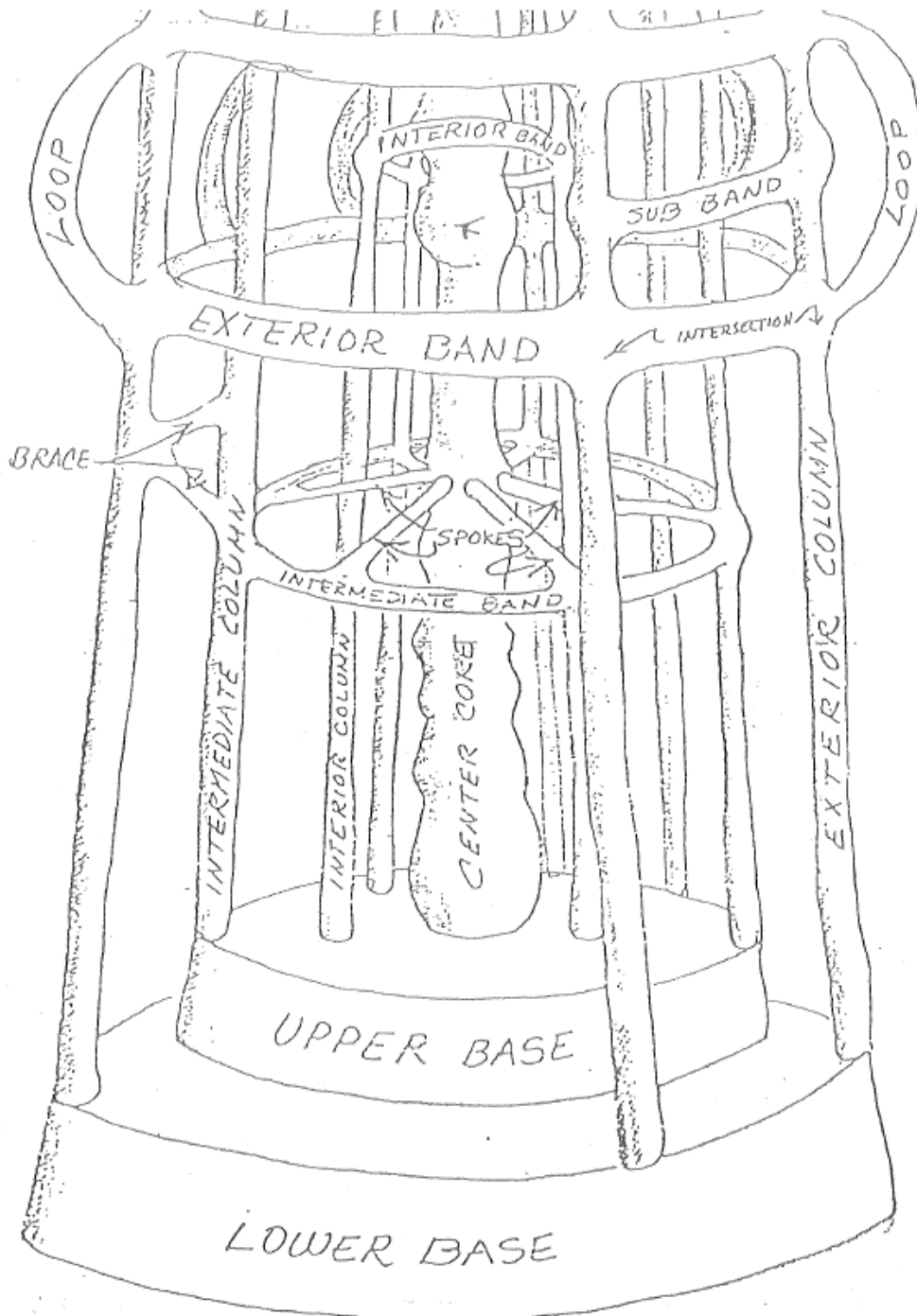


Figure 4.2: Tower member labels

The members are as follows:

- **Center Core:** large column at the center of the structure which runs vertically over the entire height
- **Columns:** Vertical members surrounded the center core, which are typically arranged in three layers (interior, intermediate and exterior).
- **Bands:** circular band surrounding the columns which help to restrain the columns and provide bracing.
- **Sub-Band:** a band that only goes around part of the tower's circumference.
- **Braces:** any member connecting two columns
- **Spokes:** any member, which connects a column to a band. These act along with the braces to provide additional stability.
- **Loops:** Any member, typically connected to an exterior column or band that arches away from the structure.

The first step for defining the geometry was to isolate the central tower from the rest of the model. It was then further subdivided into 10 sections over its height that could be defined one at a time. A number of simplifications were made in order to ease the geometry definition and model development. The typical steps and simplifications are as provided in what follows.

Steps for defining column member locations and areas:

1. A horizontal cut is made at the beginning of each one of the 10 sections.

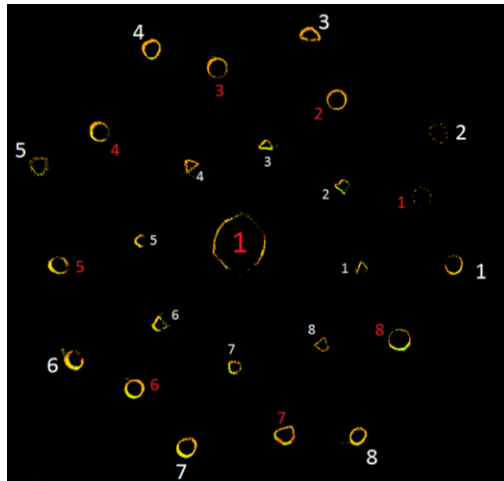


Figure 4.3: Laser scan horizontal section cut showing column locations

2. The  $(x, y)$  coordinates of the center are found for each member with the location of the center column being set to  $(0, 0)$ .
3. The radial distance and angle of each column from the center column is calculated.
4. The average radial distance to a set of exterior, intermediate, or interior columns is found and a new location for the column is calculated using the average radius and the previously calculated angle.
5. The location of the columns at any location between two sections is found by linear interpolation.
6. All columns were assumed to have a circular cross-section.

- The diameter of each column was found at the location of the cut. The average diameter of a given set (exterior, intermediate, interior) was found and uniformly applied within each section.

The following spreadsheet shows the organized data. The starting location and diameter were manually entered. The distance from the center post and new approximate location were then calculated in the spreadsheet.

Section 3													
Center Column		Starting Point			Diameter								
	x	y	z										
	545.053	513.812	5.00		0.331								
Exterior Columns		Starting Point			Diameter	Distance from center post				Approximate Location			
	x	y	z			x	y	r	$\theta$	x	error	y	error
1	546.518	513.646	5.00		0.102	1.465	-0.166	1.474	353.535	1.459	0.42%	-0.165	0.42%
2	546.350	514.653	5.00		0.111	1.297	0.841	1.546	32.960	1.232	5.02%	0.799	5.02%
3	545.517	515.214	5.00		0.099	0.464	1.402	1.477	71.688	0.461	0.59%	1.394	0.59%
4	544.419	515.122	5.00		0.109	-0.634	1.310	1.455	115.826	-0.640	-0.88%	1.322	-0.88%
5	543.669	514.295	5.00		0.107	-1.384	0.483	1.466	160.762	-1.386	-0.16%	0.484	-0.16%
6	543.906	513.050	5.00		0.109	-1.147	-0.762	1.377	213.598	-1.223	-6.61%	-0.812	-6.61%
7	544.731	512.414	5.00		0.115	-0.322	-1.398	1.435	257.029	-0.330	-2.34%	-1.431	-2.34%
8	545.843	512.519	5.00		0.095	0.790	-1.293	1.515	301.424	0.765	3.11%	-1.253	3.11%
					$D_{avg}$			$r_{avg}$	1.468				
Intermediate Columns		Starting Point			Diameter	Distance from center post				Approximate Location			
	x	y	z			x	y	r	$\theta$	x	error	y	error
1	546.300	514.124	5.00		0.122	1.247	0.312	1.285	14.047	1.221	2.10%	0.305	2.10%
2	545.785	514.862	5.00		0.106	0.732	1.050	1.280	55.118	0.720	1.68%	1.032	1.68%
3	544.918	515.018	5.00		0.113	-0.135	1.206	1.214	96.387	-0.140	-3.70%	1.251	-3.70%
4	544.043	514.574	5.00		0.109	-1.010	0.762	1.265	142.967	-1.005	0.54%	0.758	0.54%
5	543.791	513.669	5.00		0.100	-1.262	-0.143	1.270	186.465	-1.250	0.92%	-0.142	0.92%
6	544.367	512.836	5.00		0.113	-0.686	-0.976	1.193	234.898	-0.724	-5.49%	-1.030	-5.49%
7	545.359	512.546	5.00		0.084	0.306	-1.266	1.302	283.588	0.296	3.38%	-1.223	3.38%
8	546.126	513.156	5.00		0.104	1.073	-0.656	1.258	328.560	1.074	-0.06%	-0.656	-0.06%
					$D_{avg}$			$r_{avg}$	1.258				
Interior Columns		Starting Point			Diameter	Distance from center post				Approximate Location			
	x	y	z			x	y	r	$\theta$	x	error	y	error
1	546.040	513.596	5.00		0.055	0.987	-0.216	1.010	347.656	0.923	6.51%	-0.202	6.51%
2	545.894	514.278	5.00		0.085	0.841	0.466	0.961	28.991	0.826	1.76%	0.458	1.76%
3	545.283	514.679	5.00		0.064	0.230	0.867	0.897	75.143	0.242	-5.31%	0.913	-5.31%
4	544.559	514.586	5.00		0.097	-0.494	0.774	0.918	122.548	-0.508	-2.87%	0.796	-2.87%
5	544.162	513.958	5.00		0.061	-0.891	0.146	0.903	170.694	-0.932	-4.62%	0.153	-4.62%
6	544.323	513.257	5.00		0.081	-0.730	-0.555	0.917	217.245	-0.752	-3.01%	-0.572	-3.01%
7	544.916	512.867	5.00		0.061	-0.137	-0.945	0.955	261.751	-0.136	1.08%	-0.935	1.08%
8	545.632	513.003	5.00		0.076	0.579	-0.809	0.995	305.591	0.550	5.05%	-0.768	5.05%
					$D_{avg}$			$r_{avg}$	0.945				

Figure 4.4: Sample column location spreadsheet

Steps for defining the horizontal band location:

1. The horizontal bands were classified based on the set of columns which they wrapped around (exterior, intermediate, interior).
2. The height of the centroid for each band was found and then the circumference was found based on the previously defined column radial arrangement.
3. A vertical slice was made to see the cross-section of each member.
4. All horizontal bands were assumed to have a rectangular cross section.

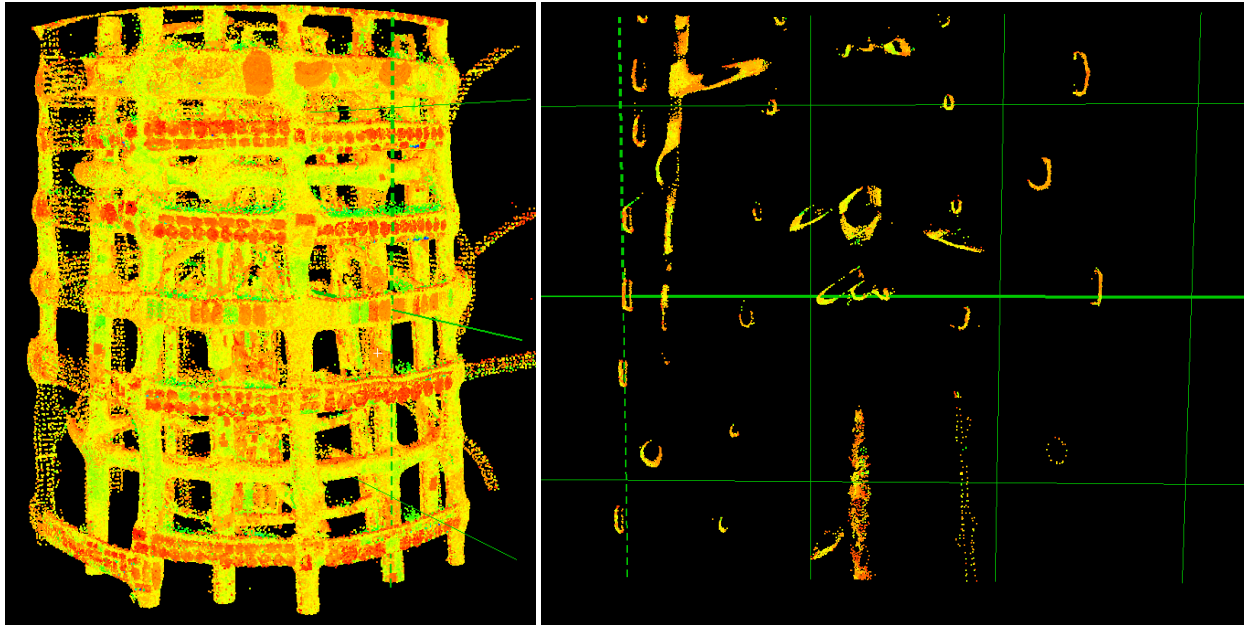


Figure 4.5: Vertical section cut showing band cross-sections

Steps for defining the spokes' locations and cross-sections:

1. Bands were assumed to be linear between the connection to the columns and the connection to the center core.
2. All spokes were assumed to have a circular cross-section.
3. The average diameter was found for each set of spokes (typically 8 members).

Using the above procedures, each member was named and given a set of nodal coordinates. These nodal coordinates were then inputted directly into Abaqus, which is a proprietary finite element modeling analysis software package (Abaqus), to define the model geometry.

### 4.3 Estimation of Structural Properties

The assumed material properties within a model can greatly impact the results. Even a model of a simple building that was constructed using modern materials will have a degree of uncertainty over the as-built material properties and overall behavior. The uncertainty is much higher for a structure as complicated as the Center Tower, built with a wide variety of materials over an extended period, and subject to deterioration and several rounds of repair over the past 60 years. The model here will first be developed using the information on reinforcement and the concrete cover that is available, and will then be updated such that the modeled behavior matches the observed behavior as closely as possible.

The Towers were constructed using an assortment of steel sections that were wrapped with a steel-wire mesh and then covered with a cement mortar. Goldstone (1963) lists two of the main structural elements used in the exterior columns of the West Tower as a 2-1/2x2-1/2x5/16 Steel Tee member, and a 2x2x1/4 Steel Angle, with cross-sectional areas of 1.62 in<sup>2</sup> and 0.944 in<sup>2</sup> respectively. Although Goldstone's tests were based on the West Tower, without any information regarding the members used in each leg of the Central Tower, the assumption was made that Rodia would have preferred using similar types and sizes of reinforcement. The approximate area of each column over the first few meters of the Central Tower is around 14 in<sup>2</sup>. Using an average of the two steel member's areas and the average cross-section yields a reinforcement ratio of 0.092.

Tests on the cement mortar reveal that it is fairly consistent with an aggregate-to-cement ratio of 2 1/4-3:1, a compressive strength of around 3000 psi, and a unit density of approximately 132.8 pcf (Ehrenkrantz, 1983). Accounting for the reinforcement, a value of 145 pcf was used as the material density—a common value for steel reinforced concrete.

ASCE 41-06, *Seismic Rehabilitation of Existing Buildings*, provides recommendations for selecting a lower-bound value of compressive strength,  $f'_c$ , when the material properties are not known.

Time Frame	Footings	Beams	Slabs	Columns	Walls
1900-1919	1000-2500	2000-3000	1500-3000	1500-3000	1000-2500
1920-1949	1500-3000	2000-3000	2000-3000	2000-4000	2000-3000
1950-1969	2500-3000	3000-4000	3000-4000	3000-6000	2500-4000
1970-Present	3000-4000	3000-5000	3000-5000	3000-10000	3000-5000

Figure 4.6: ASCE 41-06 Table 6.3. Default lower-bound compressive strength of concrete (psi)

The construction of the Towers falls almost completely in the 1920-1949 time-frame, which corresponds to a strength of around 2000-3000 psi. Initial estimates will conservatively assume a value of 2000 psi. Using the equation for modulus of elasticity in ACI 318-08 §8.5.1 yields the following for the concrete modulus of elasticity

$$E_c = w_c^{1.5} 33 \sqrt{f_c'} = (132.8)^{1.5} 33 \sqrt{2000} = 2.26 \times 10^6 \text{ psi.}$$

In the appendix of the Ehrenkrantz report, a set of calculations use a value of  $2 \times 10^6$  psi for the concrete modulus, but it is not clear where this number came from.

An equally important consideration is the amount of assumed composite action between the steel and concrete, and the amount of moment fixity assumed at each joint. For daily temperature cycle, and low-level wind or seismic events, the tower is likely to behave elastically, and therefore a high degree of composite action and fixity may be assumed. In the Goldstone test, the West Tower stayed in the linear range with no permanent offset after being loaded with a 10000-lb load that was meant to match the code level wind force (Goldstone, 1963).

In the definition of the element geometry, the gross cross-section was found. If the beam is assumed to remain in the linear-elastic range, it is more accurate to use a transformed section. The idea behind a transformed section is to convert the steel—which is significantly stiffer than concrete—to an equivalent area of concrete using the ratio of the material moduli (Hibbeler, 2008). In order to find the transformed section for the tower members, it was assumed that each section was a centrally reinforced member with a constant reinforcement ratio. The derivation of a transformed section is described next. The variables used in the said derivation are:

$r$  = radius of gross cross-section

$r_{s, \text{equiv}}$ ,  $r_{ST, \text{equiv}}$  = equivalent radius of steel section and transformed steel section

$A_g$  = gross section area

$A_s$ ,  $A_c$  = area of steel and concrete

$\rho$  = reinforcement ratio =  $A_s/A_g$

$E_s$ ,  $E_c$  = modulus of elasticity for steel and concrete

$n$  = transformation ratio =  $E_s/E_c$

$\beta$  = stiffness reduction factor (to account for cracking)

$A_{ST}$ ,  $A_T$  = transformed area of steel and total transformed area

$I_T$  = transformed moment of inertia

1) Compute the gross cross-section area and moment of inertia

$$A_g = \pi r^2$$

$$I_g = \frac{\pi r^4}{4}$$

2) Compute the area and second moment of area of steel

$$A_s = \rho A_g$$

$$r_{s,equiv} = \sqrt{\frac{\rho A_g}{\pi}} = \sqrt{\frac{\rho \pi r^2}{\pi}} = r\sqrt{\rho}$$

$$I_s = \frac{\pi r_{s,equiv}^4}{4} = \frac{\pi (r\sqrt{\rho})^4}{4} = \rho^2 \left( \frac{\pi r^4}{4} \right) = \rho^2 I_g$$

3) Compute the area and second moment of area of concrete

$$A_c = A_g - A_s = (1 - \rho)A_g$$

$$I_c = I_g - I_s = (1 - \rho^2)A_g$$

4) Compute the steel transformed area and second moment of area

$$A_{ST} = n\rho A_g$$

$$r_{ST,equiv} = \sqrt{\frac{n\rho A_g}{\pi}} = \sqrt{\frac{n\rho \pi r^2}{\pi}} = r\sqrt{n\rho}$$

$$I_{ST} = \frac{\pi r_{ST,equiv}^4}{4} = \frac{\pi (r\sqrt{n\rho})^4}{4} = (n\rho)^2 \left( \frac{\pi r^4}{4} \right) = (n\rho)^2 I_g$$

5) Compute the final transformed section properties

$$I_T = I_c + I_{ST} = \beta[1 - \rho^2 + (n\rho)^2]I_g$$

$$A_T = A_c + A_g = \beta(1 - \rho + n\rho)A_g$$

Note that the  $\beta$  term will be initially set as 1.

#### 4.4 Initial Model Results

The model was developed in Abaqus using simple wireframe geometry and two-node quadratic beam elements. The mesh was set such that each beam element was approximately 6 inches in length. With the geometry and section information for the model set, an initial modal analysis was completed in order to check how closely the frequencies matched those retrieved from the acceleration data. The results were surprisingly accurate in the N-S direction with a slightly higher E-W stiffness. In order to reduce the E-W stiffness,  $\beta$  was set to 0.5 for the beams connecting the East and Center Towers. With this correction, the frequencies matched within a reasonable error. The finished model and first two mode shapes are shown in the figure below. Table 4.1 summarizes the first three frequencies obtained from modal analysis.

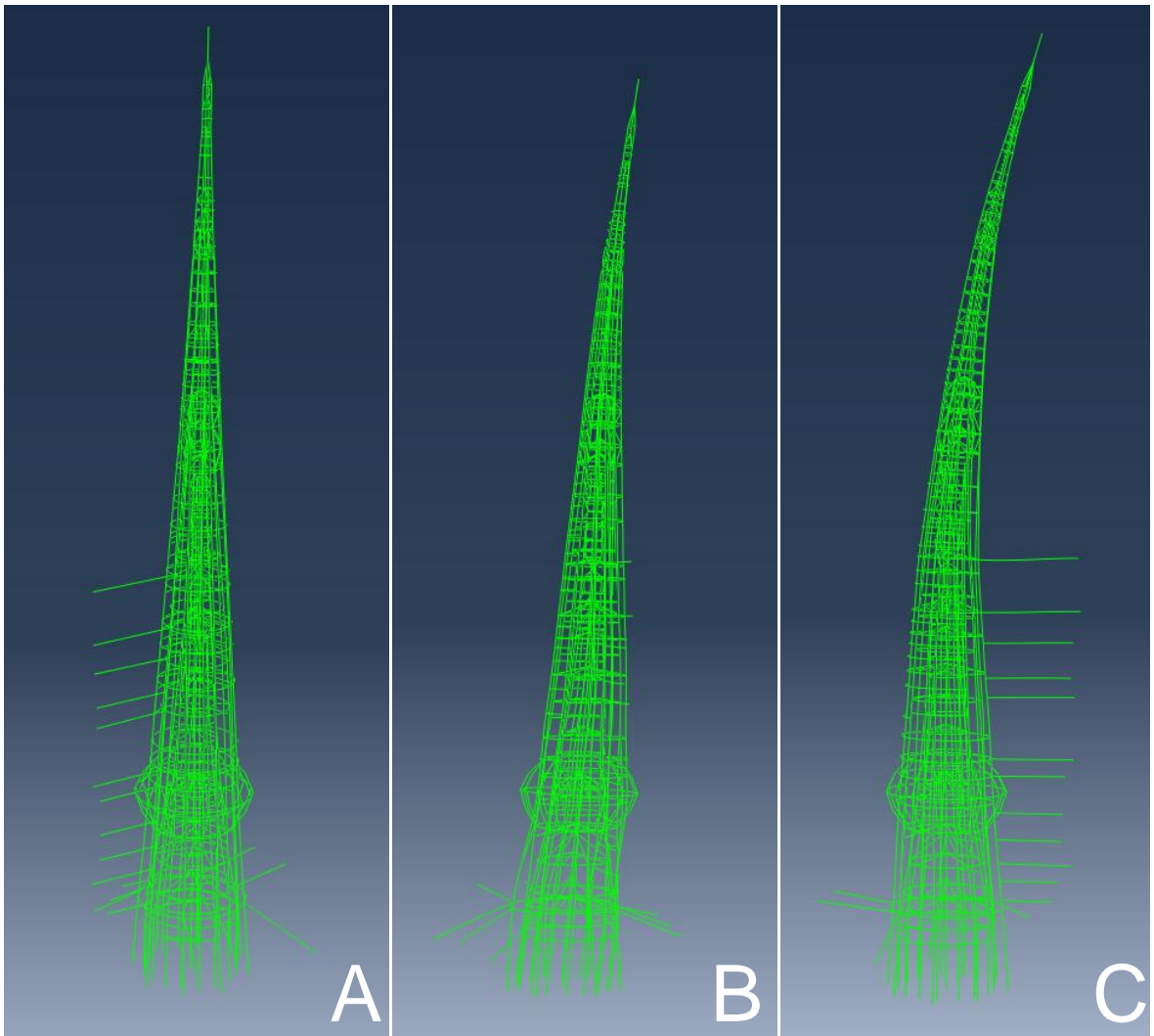


Figure 4.7: A) Finished model B) N-S first mode shape C) E-W first mode shape

Table 4.1. Comparison of ABAQUS model and measured frequencies

	North - South			East - West		
	Observed	Model	Error	Observed	Model	Error
$f_1$	2.25-2.44	2.347	-0.30%	2.31-2.65	2.943	-14.96%
$f_2$	3.54-3.97	3.205	14.08%	3.46-4.37	-	-
$f_3$	6.31-7.03	5.841	12.30%	6.75-7.49	6.679	6.06%

Note that a range of observed frequencies is given, but the percent error is the difference between the frequency in the model to the average observed frequency. In the N-S direction, where the structure isn't complicated by any coupled motion, the error in the first mode frequency is less than 1%, indicating an accurate representation of the distribution of mass and stiffness within the model. In the E-W direction the first mode error is larger, with the model overestimating the stiffness. This could possibly result from modeling the beams connecting the two towers as fixed on the east end, whereas the real condition would involve connecting the beams to another flexible structure. The second mode in the E-W direction is restrained in the model and doesn't show in the modal analysis. Again, this could be a problem with overly stiff connecting beams. The errors are nonetheless small enough that the model was deemed ready for further simulations.

#### 4.5 Thermal Simulations

The tilt of the structure in response to solar heating is an important response of the tower. Modeling this behavior may shed some light on the creation and propagation of cracks. An initial steady state simulation was completed by specifying the temperature at one side of the tower and decreasing it linearly across the width of the tower. A thermal expansion coefficient of  $1 \times 10^{-5}/^{\circ}\text{C}$  was assumed. Typical values for the thermal expansion coefficient for lightweight concrete range from  $6.5$  to  $11 \times 10^{-6}/^{\circ}\text{C}$ , while reinforcing steel has a coefficient of  $10.8 \times 10^{-6}/^{\circ}\text{C}$  (MacGregor & Wight, 2012). For the initial simulation, the gradient was set with a temperature of  $30^{\circ}\text{C}$  applied to one side of the tower, and a temperature of  $25^{\circ}\text{C}$  applied to the opposite side. The hot side was first set as the east side of the tower, and then the north, with the following results for displacement and rotation. The displacement and rotation values were taken at the nodes along the center column.

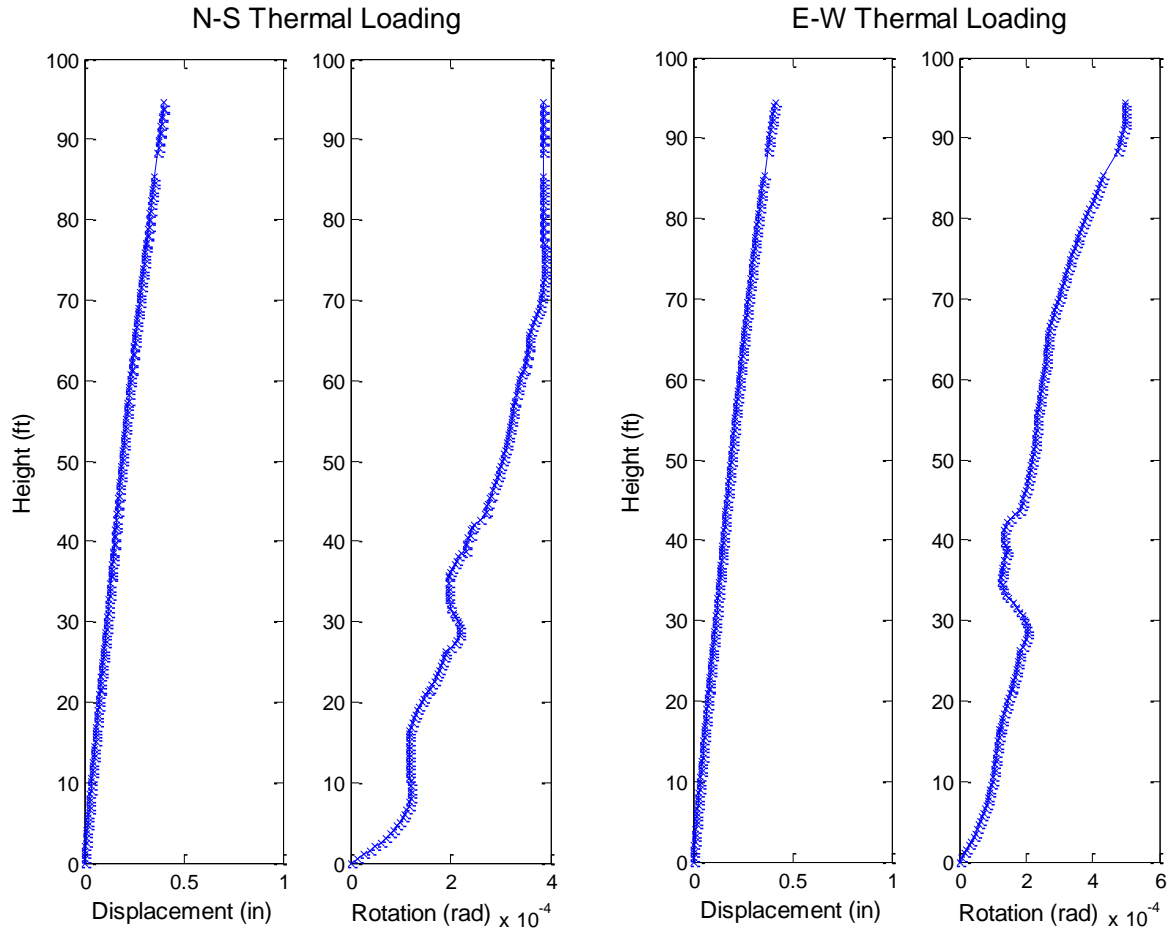


Figure 4.8: Steady state thermal displacement

In both directions, the tip displacement is around 0.5".. The rotation at 23 feet, the location of the tilt meter, is around  $2 \times 10^{-4}$  radians, meaning the peak-to-peak daily rotation would be around  $4 \times 10^{-4}$  radians. The observed values typically ranged between  $4 \times 10^{-4}$  to  $8 \times 10^{-4}$  radians. The rotation falls on the low end of the observed behavior, despite a relatively high heat input. The tip displacement for the N-S simulation was divided by the rotation at 23 feet in order to test the previously derived cantilever approximation.

$$\frac{\Delta(x)}{\theta(x)} = \frac{0.0335 \text{ feet}}{1.7 \times 10^{-4}} = 197$$

Recall that the cantilever approximation yielded a ratio of 73. The model yields a much higher displacement, which is not surprising given the decreasing flexural stiffness over the height of the tower.

The reduced rotation could result from too low of a temperature gradient. The larger the difference between the hot and cold side of the structure, the more it will tilt. The low values may also result from the surface temperature of the tower being hotter than the surrounding air. Over the course of the day, the tower stores thermal energy, causing the material to be much hotter than the surrounding air.

Future work includes modeling the tilt behavior of the tower throughout the course of the day and night. This can be accomplished using the same steady-state approach as outlined above, but in order to increase the accuracy of the results, it is necessary to better define the temperature distribution around the perimeter of the tower. A simple experiment that would involve instrumenting the tower with four or more thermometers over the course of a few days to a week will give data on the distribution of temperature that can be directly used as input for the heat simulation. The first setup should involve placing a thermometer on an exterior column in each quadrant, North, East, South and West.

With a set of known thermal loads as input the model can be further calibrated to match the observed tilt behavior. The internal stresses developed in the bands, spokes, and columns during these thermal cycles may shed light on the cause of cracks. The model may also be used to estimate the response to an earthquake or large windstorm.

## 5 Summary

The data collected from the Center Tower over the past 7 months and the UCLA analyses have provided a wealth of information on the behavior of the tower. The key findings are summarized below:

- The first mode frequency of the Center Tower is highly dependent on temperature, and can vary as much as 8% over the course of a few days.
  - An 8% change in frequency is approximately a 15% change in stiffness.
- Over the course of the day, the tower leans in response to heating from the sun. It moves in a counter clockwise ellipse each day with an approximate tip displacement of 1 to 2 inches.
  - Excessively hot temperatures may cause the tower to lean to a more extreme angle, and not fully return at the end of the day, causing long-term trends in the tilt data.
- The tower's response was recorded in one small, M4.7, earthquake. The peak acceleration was around 0.01g with a tip displacement estimated from the tilt sensor of 1.5 to 2 inches.
  - A possible shift in the south crack was seen during the earthquake.
- During a windstorm with 30+ mph gusts the recorded accelerations were approximately 50% higher than in the earthquake, but the tilt-estimated displacements were smaller.
  - Crack movement during the moderate windstorm was negligible.
- LACMA's Pi-2 sensors agree well with the UCLA sensor, and are recommended over the UB-5A sensors.
- On a daily basis, the north crack follows a pattern that is inversely proportional to the temperature.
  - The magnitude of daily movement is between 1/10000 and 1/1000 of an inch. The magnitude appears to correlate with the peak daily temperature.
- The south crack follows a bimodal daily pattern that is possibly due to its direct exposure to sunlight
  - The magnitude of daily movement for the south crack is typically around 50% higher than the movement of the north crack.
- The beam members connecting the East and Center Tower couple the motion of the two structures in the East-West direction.
  - The peak accelerations on the East Tower resulting from manual excitation of the Center Tower were 77% the accelerations recorded on the Center Tower.
  - Coupling in the North-South direction is very small.
- The damping of the Center Tower was estimated between 1-4% using the log-decrement approach.

- Modeling the Center Tower using a compressive strength for concrete of 2000 psi, a 9% reinforcement ratio, and a transformed cross-section, results in a close match between the observed fundamental frequencies and the modal frequencies in the model.
- Initial steady state thermal loading simulations are within the proper magnitude of observed behavior, but further work needs to be done in order to better define the loads.
  - Instrumenting the tower with a few thermometers can help to define an accurate set of thermal loads that can be used directly as input.

## **Acknowledgements**

We would like to thank all of the NEES interns and UCLA students who have helped with this project. Specifically we would like to thank Winston Boyce and Shushoma Sravostee for their help this summer in setting up sensors in the field and for staying on top of the data quality checks and processing. The computer model couldn't have been developed had it not been for the help of Armen Azizian, Evelyn Barkhordarian, and Homa Shahpasand in processing the laser scan. Erica Eskes, Sophia Poulos, Andrey Kozhukhovskiy and the rest of the NEES@UCLA staff make projects such as this one possible.

Our appreciation is also extended to Frank Preusser and the rest of the LACMA team for allowing us to be a part of a project with such great historical, cultural, and artistic significance.

## References

- Abaqus Unified FEA. *Abaqus Overview*. Online. <<http://www.3ds.com/products-services/simulia/portfolio/abaqus/overview/>>. [Accessed September 2013]
- ACI 318-08 (2008). *Building Code Requirements for Structural Concrete*, American Concrete Institute, Farmington Hills, MI.
- ANCO (1988). *Final Report: Simon Rodia Towers Environmental Measurements – Phase I*, prepared for the City of Los Angeles, ANCO Engineers Inc., Culver City, CA 90232, May 1988.
- ANCO (1989). *Final Report: Simon Rodia Towers Environmental Measurements – Phase II*, prepared for the City of Los Angeles, ANCO Engineers Inc., Culver City, CA 90232, April 1989.
- Applied Geomechanics. *Tiltmeter Spec Sheet*. Online. Available at: <<http://nees.org/data/get/facility/sensorModels/164/Documentation/tiltmeter%20spec%20sheet.pdf>>. [Accessed August 2013]
- ASCE/SEI (2006). *ASCE/SEI 41-06: Seismic Retrofit of Existing Buildings*, American Society of Civil Engineers, Reston, VA.
- ASCE/SEI (2006). *Supplement No.1 to ASCE 41-06: Seismic Retrofit of Existing Buildings*, American Society of Civil Engineers, Reston, VA.
- ASCE/SEI (2010). *ASCE/SEI 7-10: Minimum Design Loads of Buildings and Other Structures*, American Society of Civil Engineers, Reston, VA.
- Chopra, AK (2007). *Dynamics of Structures*, (third edition). Pearson Prentice Hall.
- The Ehrenkrantz Group/Building Conservation Technology (1983). "Preservation Plan: Simon Rodia's Towers in Watts." Los Angeles, CA
- Firstmark Controls. *World's Smallest Cable Position Transducer, Specs*. Online. Available at: <<http://www.firstmarkcontrols.com/s021f.htm>>. [Accessed August 2013]
- Hibbeler, R.C. (2008). *Mechanics of Materials, (seventh edition)*. Pearson Prentice Hall
- GBG USA. *Laser Scanning: Mobile Laser Scanner*. Online. <[http://www.gbg-us.com/#!\\_\\_laser-scanning-tech](http://www.gbg-us.com/#!__laser-scanning-tech)>. [Accessed August 2013]

Gill Instruments. *WindObserver 65: Ultrasonic Anemometer Data Sheet*. Online. Available at: <[www.gillinstruments.com/data/datasheets/WindObserver65.pdf](http://www.gillinstruments.com/data/datasheets/WindObserver65.pdf)>. [Accessed August 2013]

Goldstone B, Goldstone AP (1997). *The Los Angeles Watts Towers*, Los Angeles: Getty Conservation Institute and J. Paul Getty Museum.

Goldstone NJ (1963). *Structural Test of Hand-Built Tower*. *Experimental Mechanics*, 3(1), 8-13.

Kinematics, *Episensor ES-T Data Sheet*, Online. Available at: <<http://www.kinematics.com/uploads/PDFs/EPISENSOREST.pdf>> [Accessed August 2013]

MacGregor, James G., Wight, James K. (2012). *Reinforced Concrete: Mechanics and Design (6E)*. Pearson

MATLAB Documentation Center (2013). Online. Available at: <[www.mathworks.com/help/](http://www.mathworks.com/help/)> [Accessed August 2013]

National Oceanic and Atmospheric Administration. (2013). *LIDAR-Light Detection and Ranging*. Online. <<http://www.oceanservice.noaa.gov/facts/lidar.html>>. [Accessed September 2013]

Quanterra, *Quanterra Q330 Spec Sheet*, Online. Available at: <[www.Q330.com](http://www.Q330.com)>. [Accessed August 2013]